GCA TECHNICAL REPORT NO. 65-3-N

STUDY OF THE AVERAGE VERTICAL DISTRIBUTION OF TEMPERATURE IN THE MARTIAN ATMOSPHERE

GEORGE OHRING JOSEPH F. MARIANO

GCA CORPORATION
Bedford, Massachusetts

FINAL REPORT
NAS9-3423

PREPARED FOR

NATIONAL AERONAUTICS AND SPACE ADMINISTRATION
MANNED SPACECRAFT CENTER
HOUSTON, TEXAS

MARCH 1965

GCA Technical Report No. 65-3-N

STUDY OF THE AVERAGE VERTICAL DISTRIBUTION OF TEMPERATURE IN THE MARTIAN ATMOSPHERE

George Ohring
Joseph F. Mariano

March 1965

FINAL REPORT

Contract No. NAS9-3423

GCA CORPORATION
GCA TECHNOLOGY DIVISION
Bedford, Massachusetts

Prepared for

NATIONAL AERONAUTICS AND SPACE ADMINISTRATION
Manned Spacecraft Center
Houston, Texas

TABLE OF CONTENTS

LIST OF ILLUSTRATIONS

LIST OF TABLES

STUDY OF THE AVERAGE VERTICAL DISTRIBUTION OF TEMPERATURE IN THE MARTIAN ATMOSPHERE

By George Ohring and Joseph Mariano
GCA Corporation

SUMMARY

27955

Theoretical computations of the vertical distribution of temperature in the Martian atmosphere are performed with the use of a combined convective-radiative equilibrium model. The model assumes that the Martian troposphere is in convective equilibrium and the Martian stratosphere is in radiative equilibrium. The height of the tropopause is a by-product of the computations. Computations are performed for several physical models of the Martian atmosphere to allow evaluation of the effect of present uncertainties in such parameters as carbon dioxide content, surface pressure, tropospheric lapse-rate, surface temperature, water vapor content, and distribution of absorbing gas with height. On the basis of these calculations, a tentative model of the average vertical distribution of temperature in the Martian atmosphere is suggested. This temperature profile is based upon computations with an assumed surface pressure of 25 mb, carbon dioxide amount of 55 m STP, water vapor amount of 10^{-3} prec. cm, adiabatic lapse-rate in the troposphere, and surface temperature of 230°K. It is characterized by a tropopause at a height of about 5 km and an upper stratosphere temperature of about 145°K above 45 km.

author

INTRODUCTION

This final report covers research performed during the past six months on the average vertical distribution of temperature in the Martian atmosphere. The objective of this study is to derive estimates of the average vertical temperature profile. Since available observational indications of temperature refer only to the surface of the planet, the problem of estimating the vertical temperature structure must be approached theoretically. In the present study, a combined convective-radiative equilibrium model is used to compute the temperature profile. Atmospheric composition and surface pressures are based upon the recent observations of Kaplan, et al. *[1]. The Martian troposphere is assumed to extend to that height - the tropopause - above which radiative equilibrium leads to a stable lapse-rate. Thus, the Martian stratosphere is assumed to be in radiative equilibrium and to have a stable lapse-rate. A similar model [2] has been applied to the earth's atmosphere; the resulting temperature distributions are in good agreement with the observed temperatures. Thus, application of this model to the Martian atmosphere provides a reasonable basis for estimating the average vertical distribution of temperature.

*Numbers in [ ] throughout text indicate reference numbers.

BLANK PAGE

BACKGROUND

The concept of using a convective-equilibrium troposphere and radiative-equilibrium stratosphere model to determine the variation of temperature with altitude in the Martian atmosphere is not new. On the basis of a rough computation of the thickness of a troposphere in adiabatic equilibrium, Hess[3] estimated the height of the Martian tropopause to be about 45 km. With the assumed surface temperature of 273°K, the temperature at the tropopause is about 113°K. By assuming radiative-equilibrium for the upper atmosphere and a grey absorbing atmosphere in which absorption of solar radiation is negligible compared to absorption of infrared radiation, he computed a temperature of about 170°K for the top of the atmosphere. Thus, Hess's computations suggested that the temperature decreases at the adiabatic rate from 273°K at the surface to 113°K at the tropopause (45 km), increases with altitude from 45 km to 60 or 70 km, and then remains constant at a value of 170°K. Goody [4], using a theoretical model atmosphere characterized by adiabatic equilibrium in the troposphere and radiative equilibrium above, obtained a tropopause height of 8.5 km for an atmosphere with 2% by volume carbon dioxide, and 25 km for an atmosphere with 10^{-2} cm of precipitable water. In these computations absorption of solar radiation was neglected, and a surface temperature of 270°K and pressure of 85 mb were assumed. In the carbon dioxide model, the temperature decreases with altitude above the tropopause to about 134°K above 90 km. In the water vapor model, the stratospheric temperature decreases very little with altitude.

In a highly parameterized theoretical model, Ohring and Cote [5] investigated the variation of the height of the tropopause with different assumptions on atmospheric composition, tropospheric lapse-rate, and surface temperature. The theoretical model assumed a linear lapse-rate in the troposphere and isothermal conditions in the stratosphere. The height of the tropopause was determined from the condition that the rate of radiational temperature change at the tropopause level be zero - that is, from a condition of local radiative equilibrium at the tropopause level. The results of these computations are shown in Table 1. With carbon dioxide, at a volume percentage of 2%, as the only absorbing gas, the tropopause is located at 10 km. With 10^{-2} cm of precipitable water vapor as the only absorbing gas, the tropopause height is at 14 km. With both gases present, the tropopause height varies slightly from 12 km to 13 km as the surface temperature varies from 243°K to 283°K. If a tropospheric lapse-rate of 2.5°K/km is assumed rather than the adiabatic value of 3.7°K/km, the tropopause height is increased by about 4 km. All computations were made with a surface pressure of 85 mb and with the assumption of negligible absorption of solar radiation. Although the model is highly parameterized, the variations of tropopause height with variations in atmospheric composition, surface temperature, and tropos-

TABLE 1

TROPOPAUSE HEIGHTS (km) COMPUTED BY OHRING AND COTE (1963).

Surface Temperature (^{o}K)	Composition: Tropospheric lapse-rate (^{o}K/km)	2% CO_2 (36 m STP) 3.7	2% CO_2 (36 m STP) + 10^{-2} cm H_2O 3.7	2% CO_2 (36 m STP) + 10^{-2} cm H_2O 3.7	2% CO_2 (36 m STP) + 10^{-2} cm H_2O 2.5
283				13	18
263		10	14	12.5	17
243				12	16

pheric lapse-rate are probably qualitatively correct.

Because of the need for engineering model atmospheres for Mars, several investigators have suggested various mean and extreme temperature profiles. These profiles are based largely on assumptions of surface temperature extremes, tropopause heights, exospheric temperatures, and analogy with the earth's atmosphere. For example, Schilling [6] constructed three temperature profiles based upon surface temperatures of 200°K, 250°K, and 300°K, and corresponding tropopause heights ranging from 26 km to 10 km. As we shall see later, the height of the tropopause actually increases with increasing surface temperature. Adiabatic conditions in the troposphere and isothermal conditions in the stratosphere were assumed. Schilling also suggested a conjectural temperature profile for the Martian atmosphere. This model is based essentially upon speculation on the possible role of ozone on the Martian temperature profile and on analogy with the Earth's atmosphere. In this model, the Martian tropopause is located at 4 km. Above the tropopause, the temperature is constant up to an altitude of 40 km, where it increases to 300°K at 100 km. Aside from the fact that ozone has not been detected in the Martian atmosphere (the observed upper limit for oxygen is only 70 cm STP [1], which suggests a negligible amount of ozone - if any), Schilling's estimates of its effect on the temperature structure are purely qualitative. In a similar fashion, Evans and Wasko [7] have presented mean and extreme models of the atmospheric temperature structure on Mars. To a large extent, these are based upon assumed surface and exospheric temperatures, qualitative theoretical reasoning, and analogy with the Earth's atmosphere. These engineering models and others developed by the Jet Propulsion Laboratory and the NASA Manned Spacecraft Center have been summarized by Levin, et al. [8].

Using the convective-equilibrium troposphere and radiative-equilibrium stratosphere model, and procedures to be outlined in the next section, Ohring [9] computed the average vertical temperature distribution in the Martian atmosphere for a surface temperature of 230°K, surface pressure of 85 mb, adiabatic lapse-rate in the troposphere, and 2% by volume CO_2 content (36 m STP). Atmospheric absorption of solar radiation was neglected. The resulting temperature profile was characterized by a tropopause at about 9 km and a stratosphere with temperature continuously decreasing with height.

Recent observations by Kaplan, et al. [1] indicate higher carbon dioxide amounts and lower surface pressures on Mars than previously observed. In addition, these observations were the first in which water vapor was detected in the Martian atmosphere. It was, therefore, thought desirable to compute the vertical temperature profile using this new information. In addition, it was thought desirable to perform computations

for different combinations of surface pressure and carbon dioxide content, surface temperatures, and tropospheric lapse-rates, and also to include the effect of atmospheric absorption of solar radiation on the temperature profile. The theoretical and physical models, and the results of such computations are discussed in the next few sections.

THEORETICAL FORMULATION

Convective-Radiative Equilibrium Model

It is assumed that the most important processes controlling the vertical temperature profile in the Martian atmosphere are radiation and convection. If information is available on the composition of a planetary atmosphere, it is possible to determine the radiative equilibrium temperature profile for that atmosphere. For an atmosphere such as Mars' or the Earth's, the radiative equilibrium profile is characterized by super-adiabatic lapse-rates in the lowest layers. Such a temperature distribution is not stable; in the real atmosphere convection takes place and modifies such a temperature distribution. The effect of convection is to produce a convective-equilibrium lapse-rate in the lower layers of the atmosphere. In the Earth's atmosphere, in which water vapor condensation takes place, the lapse-rate that is established in the lower layers is closer to the moist adiabatic lapse-rate than to the dry adiabatic lapse-rate. In the Martian atmosphere, in which water vapor is scarce, the lapse-rate that is established may be close to the dry adiabatic lapse-rate. It is possible to account for this effect of convection in theoretical calculations of the vertical temperature distribution. Rather than computing a pure radiative equilibrium temperature profile, one computes a temperature profile that is characterized by two layers: a lower layer or troposphere in which the lapse-rate is equal to the convective lapse-rate, and an upper layer or stratosphere that is in radiative equilibrium and in which the lapse-rate is stable.

The concepts discussed above can be carried out as follows. Starting with an initial isothermal atmosphere whose temperature is equal to the average Martian surface temperature, one computes the radiational temperature change rates as a function of altitude. These rates are then applied to the initial temperature profile for a unit time step to obtain a new temperature profile. This process is continued until a temperature profile is obtained for which the radiational rates of temperature change are negligibly small. At each stage of the calculations, however, the temperature profiles are checked for instability; if any layer has a lapse-rate greater than the convective lapse-rate, the temperatures are brought back to the convective lapse-rate prior to the next calculation of radiational rates of temperature change. Throughout the computations, the surface temperature is held constant. Within the limits of the theoretical formulation, the final temperature profile obtained from such calculations should be representative of actual conditions in the Martian atmosphere.

Infrared Cooling

Infrared cooling rates are determined from the divergence of the net flux of infrared radiation with height, as computed with the aid of Elsasser's [10] radiation tables. A sample calculation, described in Section 5, comparing carbon dioxide and water vapor cooling rates, suggests that infrared cooling in the Martian atmosphere is controlled by carbon dioxide. Thus, only the 15μ carbon dioxide band is considered in the infrared cooling computations.

Following Elsasser's (1960) notation, the upward and downward fluxes of radiation at any reference level can be written as

$$F \uparrow (0) = \sigma T_g^4 - \int_{T_0}^{T_g} R(u,T)dT \qquad (1)$$

$$F \downarrow (0) = \int_{T_1}^{T_0} R(u,T)dT + \int_{0}^{T_1} R(u_1,T)dT \qquad (2)$$

where

$$R(u,T) = \int_{\Delta\nu} (dB_\nu/dT)\,[1 - \tau_P(u)]d\nu \qquad (3)$$

where $F \uparrow (0)$ and $F \downarrow (0)$ are the upward and downward radiation fluxes at the reference level, σ is the Stefan-Boltzmann constant, T_g is the ground temperature, u is the reduced carbon dioxide path length (measured in cm STP and increasing upwards and downwards from the reference level), T is temperature, T_1 is the temperature at the top of the atmosphere, T_0 is the temperature at the reference level, u_1 is the reduced carbon dioxide path length from the top of the atmosphere to the reference level, B_ν is the blackbody energy per unit spectral interval, and τ is the flux transmissivity. Elsasser's [10] radiation tables list R as a function of log u and T. The integral in Equation (1) and the first integral in Equation (2) follow the actual temperature-path-length relationship in the atmosphere; the second integral in Equation (2) is a boundary term; the integral in Equation (3) extends over the wave number range $\Delta\nu$ covered by the gaseous absorption band. The derivations of equations (1) and (2) are presented in Appendix A.

The net flux at any level is given by the difference between the upward and downward fluxes.

$$F_{net}(0) = F \uparrow (0) - F \downarrow (0) \qquad (4)$$

The radiational rate of temperature change can be obtained from the vertical divergence of the net flux

$$\frac{\Delta T}{\Delta t} = \frac{g}{c_p} \frac{\Delta F_{net}}{\Delta p} \tag{5}$$

where $\Delta T/\Delta t$ is the radiational rate of temperature change for a layer of pressure thickness Δp, g is the acceleration of gravity, and c_p is the specific heat of the atmosphere at constant pressure.

The atmospheric integrals in Equations (1) and (2) are computed numerically by dividing the atmosphere into n layers of constant pressure thickness. In most cases, a 20-layer model is used. The temperature of each layer is taken as the average of the temperatures at the base and top of the layer and is assumed to apply at the mid-point of the layer. The reduced path lengths, except for u_1, are measured from the reference level to the mid-point of each layer; u_1 is measured from the reference level to the top of the atmosphere. The boundary integral in Equation (2) is also evaluated numerically with the use of 20 intervals and the trapezoidal rule. Elsasser's R(u,T) table consists of values of R(u,T) tabulated at intervals of 10°C in temperature and 0.3 or 0.4 in log u; linear interpolation is used to determine values of R(u,T) between tabulated values. The surface temperature is held constant throughout the iteration process; the temperature at the top of the atmosphere is linearly extrapolated from the temperatures at the mid-point and base of the top-most layer of the model. The calculations are continued until all of the radiational rates of temperature change - except in the convective layer - are less than 0.05°K/day.

Solar Heating

Heating due to atmospheric absorption of solar radiation by the near infrared bands of carbon dioxide and water vapor is computed using the method of Roach [11], which is based upon the experimental absorption data of Howard et al. [12]. Following Roach [11], the amount of solar energy absorbed from a pressure level p to the top of the atmosphere can be written as

$$E = \sum_i I_{oi} \cos \psi A_i$$

where I_{oi} is the intensity of solar radiation per wave number at the top of the atmosphere in the i^{th} absorption band, ψ is the solar zenith angle, A_i is the absorptivity per wave number of the i^{th} band for the atmospheric column extending from the top of the atmosphere to the pressure level p along a slant path parallel to the solar beam, and the summation extends over the carbon dioxide and water vapor absorption bands. The heating rate at a pressure level p can be determined from

$$\frac{dT}{dt} = \frac{g}{c_p} \cos \psi \sum_i I_{oi} \frac{dA_i}{dp}$$

The absorptivity A_i is a function of m (sec ψ), the amount of absorber in the slant path through the atmosphere, and $\bar{p}$, the effective pressure of the atmosphere above the level p, which, according to the Curtis-Godson approximation, is given by $\int p\, dm / \int dm$. If the absorbing gas has a constant mixing ratio with altitude, the effective pressure is simply the average pressure of the atmosphere above the level p. One can write

$$\frac{dA_i}{dp} = \frac{\partial A_i}{\partial m} \frac{dm}{dp} + \frac{\partial A_i}{\partial \bar{p}} \frac{d\bar{p}}{dp}$$

The values of $\frac{dA_i}{dp}$ can be computed from the empirical equations of Howard et al. [12], which relate A_i to m and $\bar{p}$ for the various bands. They present two different absorption laws, which we rewrite slightly to apply to the present problem of slant path absorption in a real atmosphere.

Weak absorption bands

$$A = c\ (m \sec \psi)^{\frac{1}{2}}\ (\bar{p})^k \text{ for } A < A_c$$

Strong absorption bands

$$A = C + D \log (m \sec \psi) + K \log \bar{p} \text{ for } A \geq A_c$$

where c, k, C, D, and K are empirically determined constants, and A_c is the critical value of the absorptivity at which the absorption changes from weak to strong. The empirical constants for the carbon dioxide and water vapor bands are listed in Table 2. These values are taken from Roach [11]; the values in parentheses have been altered from the original Howard et al. [12] data as explained by Roach [11]. These constants are appropriate for $\bar{p}$ measured in mm of mercury, and m in cm STP for carbon dioxide and in precipitable cm for water vapor. To simplify the present computations a value of k = 0.4 was assumed for all the carbon dioxide bands, and k = 0.3 for all the water vapor bands. For the small amounts of water vapor in the Martian atmosphere, the weak absorption law applies to all the water vapor bands.

The values of I_o tabulated in Table 2 are solar radiation intensities at the top of the Martian atmosphere. Since, during an average day on Mars, the sun shines one-half of the time, the average value of I_o is simply $I_o/2$. The average value of cos ψ is 0.5. These values are used in the computations of the average solar heating rates. The solar heating rates are computed for the mid-points of each of the n layers into which the atmosphere is divided.

TABLE 2

EMPIRICAL CONSTANTS FOR ABSORPTION BANDS

Band $\lambda(\mu)$ CO_2	c	k	C	D	K	A_c cm^{-1}	I_o erg cm^{-2} sec^{-1} (wave number)$^{-1}$
1.4	0.058	0.41				80	27.4
1.6	0.063	0.38				80	24.6
2.0	0.492	0.39	(-548)	138	114	80	18.6
2.7	3.15	0.43	(-137)	77	68	50	12.0
4.3	-	-	27.5	34	31.5	50	5.68
4.8	0.12	0.37	-	-	-	60	4.77
5.2	0.024	0.40	-	-	-	30	4.13
$\lambda(\mu)$ H_2O							
0.94	38	0.27	(-135)	(230)	(125)	(200)	31.2
1.1	(42)	0.26	(-292)	(345)	(180)	(300)	31.0
1.38	163	0.30	(251)	460	198	350	27.6
1.87	152	0.30	(143)	232	144	275	20.1
2.7	316	0.32	(316)	246	150	200	12.0
3.2	40.2	0.30	(-144)	295	151	250	9.03
6.3	356	0.30	302	218	157	160	3.01

Computational Techniques

The vertical temperature distribution for a given surface temperature and pressure is found when the resulting radiative flux divergence, $\frac{dF}{dz}$, is zero throughout the radiative equilibrium layer. This temperature distribution is obtained numerically by dividing the atmosphere into n layers of pressure thickness Δp (see Fig. 1), and solving the finite difference equation,

$$\frac{\Delta T_i}{\Delta t} = \frac{-g}{c_p} \frac{\Delta F_i}{\Delta p} + S_i = 0 , \quad (i=1,2,\ldots,n) \tag{6}$$

where $\frac{\Delta T_i}{\Delta t}$ is the rate of change of temperature at the mid-point of the i th layer, ΔF_i is the net infrared flux at the upper boundary minus the net infrared flux at the lower boundary of the i th layer, g is the acceleration due to gravity, c_p is the specific heat at constant pressure and S_i is the solar heating rate for the i^{th} layer. The pressure thickness Δp is always taken as a positive quantity.

Equation (6) is solved by an iteration procedure. Beginning with an initial temperature profile, $(T_1, T_2, \ldots, T_n)$, the upward and downward radiation fluxes at the boundaries of each layer, $F_k \uparrow$ and $F_k \downarrow$ respectively, $(k=1,2,\ldots,n+1)$, are obtained by approximating Equations (1) and (2) in the following manner. Each layer in the atmosphere has a reduced carbon dioxide path length Δu_i $(i=1,2,\ldots,n)$. The integral in Equation (1), where the reference level is the k^{th} boundary, is approximated as,

$$\int_{T_o\ (k^{th}\ \text{boundary})}^{T_g} R(u,T)\,dT \approx \sum_{i=1}^{k-1} R(u_{\underline{k},i}, T_i)\nabla T_i \tag{7}$$

where $u_{\underline{k},i}$ is the reduced carbon dioxide path length between the k^{th} boundary and the mid-point of the i^{th} layer, and ∇T_i is the temperature at the lower boundary minus the temperature at the upper boundary of the i^{th} layer.

$$\nabla T_i = \begin{cases} \frac{1}{2}(T_{i-1} + T_i) - \frac{1}{2}(T_i + T_{i+1}) = \frac{1}{2}(T_{i-1} - T_{i+1}), & i=2,3,\ldots,n-1, \\ T_g - \frac{1}{2}(T_1 + T_2), & i=1 , \\ T_{n-1} - T_n , & i=n . \end{cases} \tag{8}$$

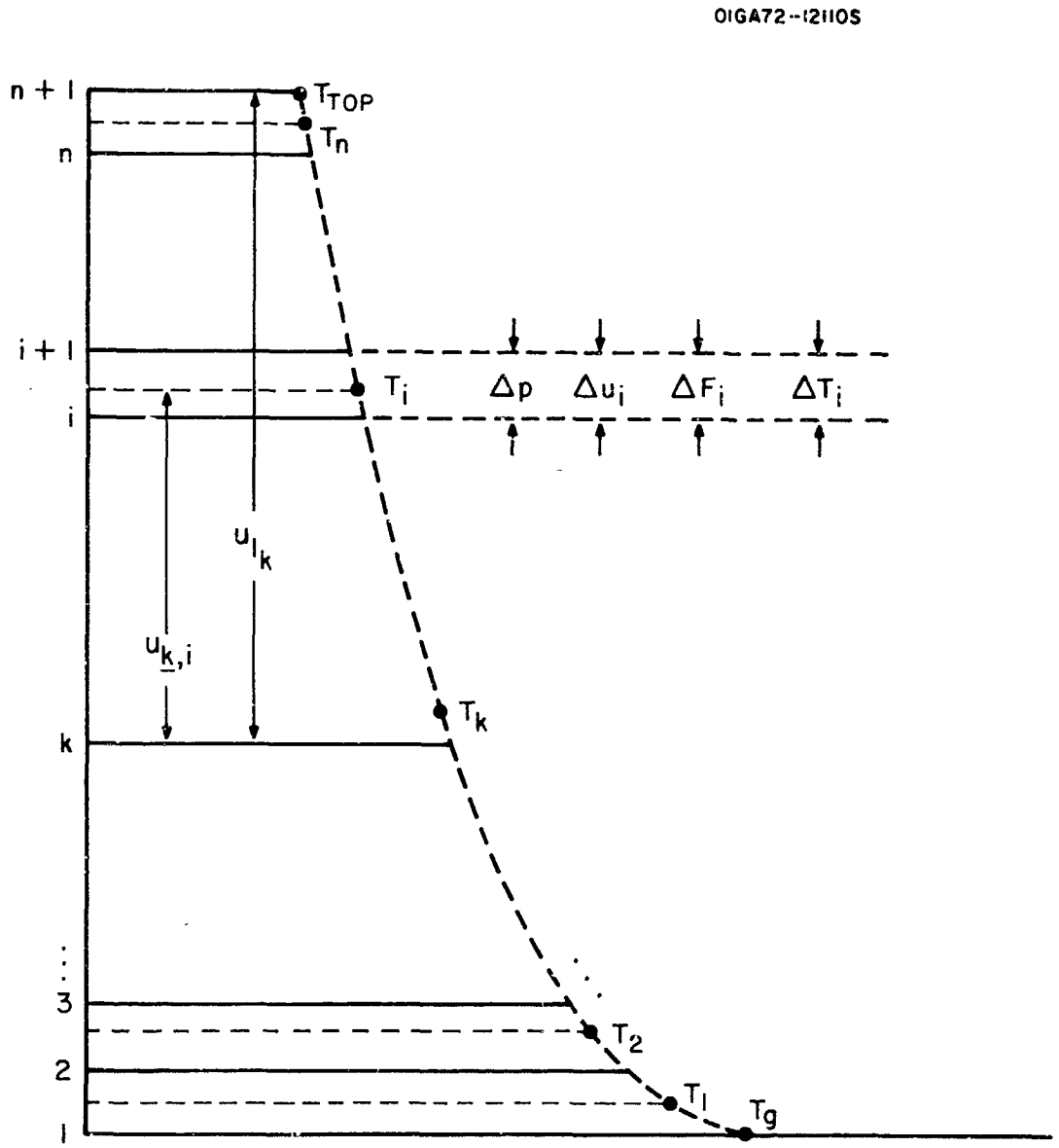

Figure 1. Schematic diagram of division of the atmosphere into n layers for numerical calculations.

$$u_{\underline{k}} = \Delta u_{k-1} + \Delta u_{k-2} + \ldots + \Delta u_{i+1} + \frac{1}{2}\Delta u_i \qquad (9)$$

The first integral of Equation (2) is approximated as,

$$\int_{T_1}^{T_o(k^{th}\ \text{boundary})} R(u,T)dT \approx \sum_{i=k}^{n} R(u_{\underline{k},i}, T_i)\nabla T_i \quad , \qquad (10)$$

where ∇T_i is given by (8) and,

$$u_{\underline{k},i} = \Delta u_k + \Delta u_{k+1} + \ldots + \Delta u_{i-1} + \frac{1}{2}\Delta u_i \quad . \qquad (11)$$

The temperature at the top of the atmosphere, T_{top}, is obtained by a linear extrapolation of T_n and T_{n-1}.

The second integral in (2) is evaluated by integrating with the trapezoidal rule from 73 degrees Kelvin to T_{top}. (This integration is performed from 73°K rather than from 0°K because all values of R used in this study are equal to zero to three places for T < 73°K.)

$$\int_{0}^{T_1} R(u_{1_k}, T)dt \approx \sum_{i=1}^{20} R(u_{1_k}, T'_i)\nabla T'_i \qquad (12)$$

where u_{1_k} is the reduced carbon dioxide path length between the k^{th} boundary and the top of the atmosphere,

$$u_{1_k} = \Delta u_k + \Delta u_{k+1} + \ldots + \Delta u_n \quad , \qquad (13)$$

$$T'_i = 73 + \frac{(T_{top} - 73)}{20} \times i \quad . \quad (i=1,2,\ldots,20) \qquad (14)$$

where

$$T'_{20} = T_{top} \quad ,$$

and,

$$\nabla T'_1 = \begin{cases} \frac{1}{2}(T'_1 - 73) & , \quad i=1 \\ T'_i - T'_{i-1} & , \quad i=2,3,\ldots,19 \\ \frac{1}{2}(T'_{20} - T'_{19}) & , \quad i=20 \end{cases} \qquad (15)$$

Therefore, the net flux at the k^{th} boundary is,

$$F_{net}(k) = F_k\uparrow - F_k\downarrow = \sigma T_g^4 - \sum_{i=1}^{n} R(u_{\underline{k},i}, T_i)\nabla T_i - \sum_{i=1}^{20} R(u_{1_k}, T_i')\nabla T_i' \quad , \qquad (16)$$

and the flux divergence of the i^{th} layer is,

$$\Delta F_i = F_{net}(i+1) - F_{net}(i) \quad , \qquad (i=1,2,\ldots,n) \quad . \qquad (17)$$

For a given time interval $\Delta t'$, the change in temperature for each layer, $\Delta T_i'$, is computed by multiplying the rate of temperature given by Equation (6) by $\Delta t_i'$, and the new temperature profile becomes,

$$T_i^* = T_i + \Delta T_i' \quad , \qquad (i=1,2,\ldots,n) \quad . \qquad (18)$$

Finally, the differences between the temperature at each layer, T_i^*, and the adjacent upper layer, T_{i+1}^*, are compared with the adiabatic temperature lapse-rate to insure that no temperature differences exceed the corresponding adiabatic temperature differences. If a temperature difference (say, $T_{i+1}^* - T_i^*$) does exceed the adiabatic temperature difference, the upper temperature, T_{i+1}^*, is replaced by the adiabatic temperature,

$$T_{i+1}^* = T_i^* \left(\frac{p_{i+1}}{p_i} \right)^{\frac{\gamma-1}{\gamma}} \qquad (19)$$

where p_i and p_{i+1} are the pressures at the mid-points of the i^{th} and $(i+1)^{th}$ layers respectively. This ends the iteration cycle, and the new adiabatically corrected temperature profile becomes the initial temperature profile of the next cycle. The iteration process is continued until the rate of change of temperatures at each layer, $(\Delta T_i/\Delta t)$, are less than .05 degrees per day. A program which performs these calculations has been constructed, and is appended to this report. After the first calculations, the number of iterations was considerably reduced by using as an initial temperature profile a guess based upon the results of the first calculations. In these calculations, the quantities, R(u,T), as defined by Equation (3), varied from T = 73°K to T = 300°K and from log u = -2 + .7 to log u = +2.7. Some of these values were obtained from Elsasser's tables, [10], and the remaining R's were computed by evaluating the integral of Equation (3) by Simpson's rule over the range, ν = 555 cm^{-1} to 815 cm^{-1}. dB_ν/dT is computed analytically from the derivative of the Planck function. The flux transmissivity, τ_F, is evaluated from the equation,

$$\tau_F(u,\nu,T) = \tau_F[\log u + \log L(\nu,T)] \qquad (20)$$

where $L(\nu)$, the generalized absorption coefficient [10] is obtained from the equation,

$$\log[L(\nu,T)] = \log[L_o(\nu)] + \Delta\log[L(\nu,T)] \quad . \tag{21}$$

$$\Delta \log[L(\nu,T)] = \begin{cases} -4.6 \times 10^{-4} \frac{(293-T)}{T} (\nu-670)^2 + \log \frac{293}{T} , & \nu < 670 \text{ cm}^{-1} \\ -3.4 \times 10^{-4} \frac{(293-T)}{T} (\nu-670)^2 + \log \frac{293}{T} , & \nu > 670 \text{ cm}^{-1} \end{cases} \tag{22}$$

and $\log[L_o(\nu)]$ is tabulated in Elsasser's report [10].

The computed values of $R(u,T)$ differ from the measured values by a correction factor, A/A_1, which is given in Elsasser's report [10]. However, it was found to be more accurate to make this correction by multiplying the computed R's by the quantity $C(u)/C_1(u)$, where $C(u)$ is the average value of R for a given u, over the range T = 193°K to T = 300°K, obtained from Elsasser's table for R (Elsasser, 1960), and $C_1(u)$ is the corresponding average value of the computed R's.

These calculations have been programed as a second program, which is appended to this report; values of $R(u,T)$, for T = 73°K to 193°K, log u = -2 + .7 to log u = +2.7 are shown in Table 3.

The iteration program, discussed above, calculates the temperature at the mid-point of each layer, T_i, as a function of p, the pressure at that point. The resulting T-p coordinate system can be transformed to a temperature-height, T-Z, coordinate system as follows.

1. In the convective region, T varies linearly with height according to the convective lapse-rate, α.

Therefore

$$Z_i = \frac{T_i - T_g}{\alpha} \tag{23}$$

In the radiative equilibrium region, the hydrostatic equation can be be written as

$$\frac{dp}{p} = - \frac{mg}{R^* T} dZ \tag{24}$$

where m is the molecular weight of the atmosphere, and R^* is the universal gas constant.

T can be written as

$$T = T_i - \beta(p_i - p) \tag{25}$$

TABLE 3

R[log u, T] FOR CARBON DIOXIDE
(T in °C)

log u	-200°	-190°	-180°	-170°	-160°	-150°	-140°	-130°	-120°	-110°	-100°	-90°	-80°
-2+.7	0.000	0.000	0.001	0.003	0.006	0.011	0.017	0.025	0.034	0.044	0.056	0.068	0.082
-1	0.000	0.000	0.002	0.004	0.009	0.015	0.024	0.035	0.048	0.063	0.080	0.098	0.117
-1+.3	0.000	0.000	0.002	0.006	0.012	0.020	0.032	0.047	0.065	0.086	0.109	0.134	0.162
-1+.7	0.000	0.001	0.003	0.008	0.017	0.028	0.045	0.067	0.092	0.123	0.155	0.191	0.233
0	0.000	0.001	0.004	0.010	0.020	0.035	0.056	0.082	0.114	0.151	0.192	0.237	0.288
.3	0.000	0.001	0.005	0.012	0.024	0.041	0.066	0.096	0.134	0.178	0.227	0.281	0.342
.7	0.000	0.002	0.006	0.014	0.028	0.049	0.078	0.115	0.160	0.213	0.273	0.339	0.412
1	0.000	0.002	0.007	0.016	0.031	0.055	0.088	0.129	0.179	0.239	0.306	0.381	0.463
1.3	0.000	0.002	0.007	0.017	0.034	0.060	0.095	0.141	0.197	0.263	0.338	0.421	0.513
1.7	0.000	0.002	0.008	0.019	0.038	0.067	0.107	0.158	0.221	0.296	0.380	0.474	0.578
2	0.000	0.003	0.009	0.020	0.041	0.072	0.115	0.171	0.239	0.320	0.412	0.513	0.626
2.3	0.000	0.003	0.009	0.022	0.044	0.077	0.124	0.183	0.256	0.343	0.442	0.552	0.673
2.7	0.000	0.003	0.010	0.024	0.048	0.084	0.134	0.199	0.279	0.374	0.482	0.603	0.735

where $\beta = \frac{dT}{dp}$, which is assumed constant between any two temperatures T_i and T_{i+1}. Substituting (25) into (24), we have

$$\frac{dp}{p} = -\frac{mg\ dz}{R^*[T_i - \beta(p_i - p)]} \tag{26}$$

Integrating from p_i to p_{i+1}, and setting $\beta = \frac{(T_i - T_{i+1})}{(p_i - p_{i+1})}$ we find

$$Z_{i+1} = Z_i + \frac{R^*}{mg}\left\{(T_i - T_{i+1}) - \left[T_i - p_i \frac{(T_i - T_{i+1})}{(p_i - p_{i+1})}\right] \ln \frac{p_{i+1}}{p_i}\right\} \tag{27}$$

Appended to this report is a program to perform these calculations.

PHYSICAL MODELS

To compute the temperature distribution, physical models of the atmosphere are required. These models specify the assumed atmospheric composition, pressure, gravitational acceleration and surface temperature. The amounts of absorbing gases, adiabatic lapse rates, and thermodynamic constants are derived from the assumed physical models. Since there is presently some uncertainty in the actual physical model, computations are performed for several physical models.

Composition and Surface Pressure

The assumed atmospheric compositions are based largely upon the measurements of Kaplan, et al. [1]. Their measurements indicate that the carbon dioxide mass percentage in the Martian atmosphere is 16%, the surface pressure is 25 mb, and the total amount of water vapor is about 14μ precipitable water. Because of the uncertainties in their measurements, they also indicate two extreme atmospheres: CO_2 mass percentage equal to 7.5%, surface pressure equal to 40 mb; and CO_2 mass percentage equal to 60%, surface pressure equal to 10 mb. One other composition model was used. This model is based upon the previous estimates of composition and surface pressure; it assumes a CO_2 mass percentage of 3.1% and surface pressure of 85 mb. In all the models, it is assumed that nitrogen is the only other gas in the Martian atmosphere.

The mean molecular weight of each model atmosphere can be computed from

$$\frac{1}{m} = \left(CO_2\ M\%\right) \frac{1}{m_{CO_2}} + \left(N_2\ M\%\right) \frac{1}{m_{N_2}}$$

where m is the mean molecular weight, CO_2 M% is the mass percentage of CO_2, N_2 M% is the mass percentage of nitrogen, m_{CO_2} is the molecular weight of CO_2, and m_{N_2} is the molecular weight of nitrogen.

The unreduced CO_2 path length can be computed from

$$u' = \left(CO_2\ M\%\right)\ p_g/g\ \rho'_{CO_2}$$

where u' is the unreduced CO_2 path length, CO_2 M% is the mass percentage of CO_2, p_s is the Martian surface pressure, g is the Martian acceleration

of gravity (373 cm/sec^2), and ρ'_{CO_2} is the density of carbon dioxide at standard temperature and pressure (1.94×10^{-3} g/cm^3).

In those computations in which the effect of absorption of solar radiation by water vapor is investigated, water vapor amounts of 10^{-2} and 10^{-3} cm precipitable water are used.

In all computations except one, the absorbing gases are assumed to be uniformly distributed with height. In the computations of infrared cooling rates, a linear pressure correction ($\bar{p}/1000$, where $\bar{p}$ is the average pressure in mb) is applied to all path lengths to account for pressure broadening of the absorption lines. The pressure correction for the computations of solar heating rates is discussed in a previous section.

Thermodynamic Constants

The adiabatic relationship between temperature and pressure is given by

$$\left(\frac{T_2}{T_1}\right) = \left(\frac{p_2}{p_1}\right)^{\frac{\gamma-1}{\gamma}}$$

where T is temperature; p is pressure; $\gamma = c_p/c_v$, the ratio of the specific heat at constant pressure to the specific heat at constant volume; and the subscripts 1 and 2 refer to two different levels in the atmosphere. Both γ and c_p (which is required for the computation of the rates of radiational temperature change) depend mainly on atmospheric composition, although there is also a slight variation of these parameters with temperature and pressure. For a Martian atmosphere consisting of a mixture of nitrogen and carbon dioxide, γ and c_p can be determined from

$$\gamma = (N_2\ M\%)\ \gamma_{N_2} + (CO_2\ M\%)\ \gamma_{CO_2}$$

and

$$c_p = (N_2\ M\%)\ c_{p_{N_2}} + (CO_2\ M\%)\ c_{p_{CO_2}}$$

The variation of γ and c_p with temperature and pressure is so small that it is sufficient to take their values at some average temperature and pressure for the Martian atmosphere. For all models except the one with a surface temperature of 300°K, a temperature of 200°K and pressure of 10 mb were used for the evaluation of γ and c_p. For the model with a surface temperature of 300°K, a temperature of 270°K rather than 200°K was used for the evaluation of γ and c_p. Values of γ and c_p for nitrogen and carbon dioxide at these temperatures and pressures were obtained from Hilsenrath, et al. [13].

The assumed physical models for which temperature profiles were computed are summarized in Table 4. The reasons for investigating the behavior of each of these physical models is discussed in the next section.

TABLE 4

PHYSICAL MODELS USED IN COMPUTATIONS OF VERTICAL TEMPERATURE DISTRIBUTION

Models in which Solar Heating is Neglected

Model Number	p_g (mb)	u'_{CO_2} (m STP)	u'_{H_2O} (prec. cm)	$\frac{\gamma-1}{\gamma}$	c_p (cal/g deg)	T_g (^oK)
1	25	55	0	.281	.237	230
2	85	36	0	.285	.247	230
3	40	41	0	.284	.243	230
4	10	83	0	.269	.205	230
5	25	55	0	.281	.237	200
6	25	55	0	.278	.240	300
7	25	55	0	.182	.237	230
8	25	55*	0	.281	.237	230

Models in which Solar Heating is Included

Model Number	p_g (mb)	u'_{CO_2} (m STP)	u'_{H_2O} (prec. cm)	$\frac{\gamma-1}{\gamma}$	c_p (cal/g deg)	T_g (^oK)
9	25	55	0	.281	.237	230
10	25	55	10^{-3}	.281	.237	230
11	25	55	10^{-2}	.281	.237	230

*In this model, the CO_2 mixing ratio decreases by one order of magnitude from the lowest atmospheric layer to the highest layer.

RESULTS

The computed temperature profiles are presented in graphical form in this section, with the ratio of pressure to surface pressure and height as the vertical coordinate. The height of the tropopause is indicated by a short horizontal bar in the graphs. In Appendix B, the computed temperatures are tabulated as a function of pressure and height.

The first four figures illustrate the effect of different carbon dioxide contents and surface pressures on the computed profiles. In these computations, a surface temperature of 230°K and an adiabatic troposphere are assumed and solar heating is neglected. The four profiles are remarkably similar. There is only a 4°K difference in the temperature of the highest layer, with the highest temperature, 129°K, occurring in the 10-mb model and the lowest temperature, 125°K, in the 85-mb model. The similarity in the computed profiles is due to the fact that the infrared absorption is a function of the product of the carbon dioxide content and the average pressure. In the four models, an increase in surface pressure is associated with a decrease in carbon dioxide content. Thus, despite the eight-fold variation in surface pressure among the four models, there is only about a factor of four difference in the reduced path lengths, with the 85-mb case having the highest and the 10-mb case the lowest reduced path lengths. Apparently, a factor of four in reduced path length is not large enough to produce substantial changes in the computed temperature profiles. The height of the tropopause varies slightly among the four models, being less than 7 km for the two higher pressure models and greater than 7 km for the two lower pressure models. Thus, both the temperature in the uppermost layer and the height of the tropopause increase slightly as the reduced carbon dioxide path length decreases by a factor of four. However, these variations are small and suggest that the Martian temperature profile is not particularly sensitive to the uncertainties in present estimates of carbon dioxide amounts and surface pressures.

In the 10-mb case, it was not possible to obtain a final temperature profile in which all the rates of radiational temperature change were less than 0.05°C/day. The rate of temperature change is inversely proportional to the pressure thickness of a layer. Thus, to have achieved the criterion of 0.05°C/day in the 10-mb case, in which each layer is only $\frac{1}{2}$ mb thick, would have required much greater accuracy in the computations of the fluxes of radiation. The radiation tables and interpolation procedures used are apparently not sufficiently refined to provide the required accuracy. Therefore, a cut-off value of 0.1°C/day was used in the 10-mb case. If ten layers rather than twenty layers are used in the 10-mb case, it is possible to achieve the criterion of 0.05°C/day. The computed final profile using ten layers and a cutoff of 0.05°C/day is substantially the same as for twenty layers and a cutoff of 0.1°C/day.

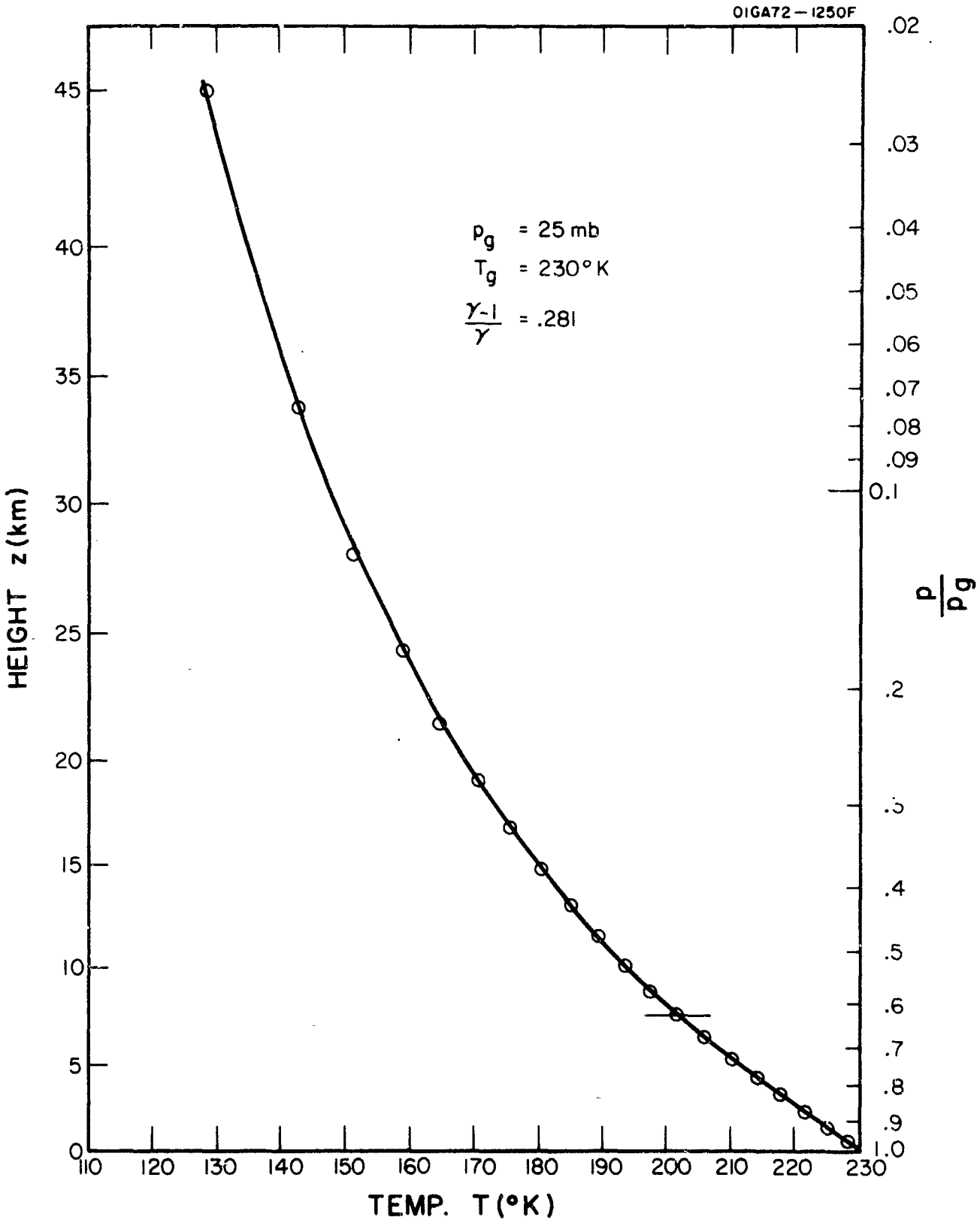

Figure 2. Vertical distribution of temperature in the Martian atmosphere (Physical Model 1).

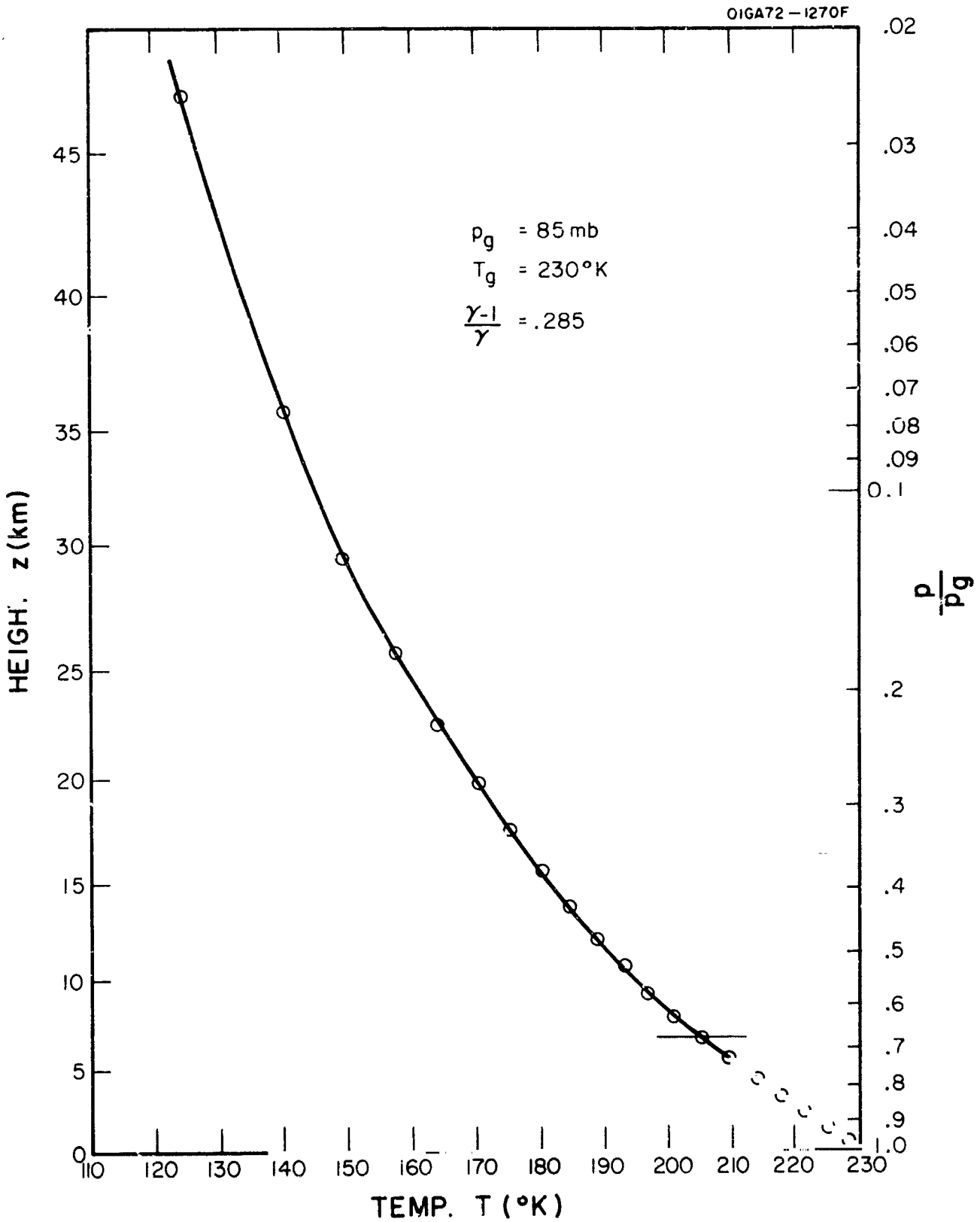

Figure 3. Vertical distribution of temperature in the Martian atmosphere (Physical Model 2).

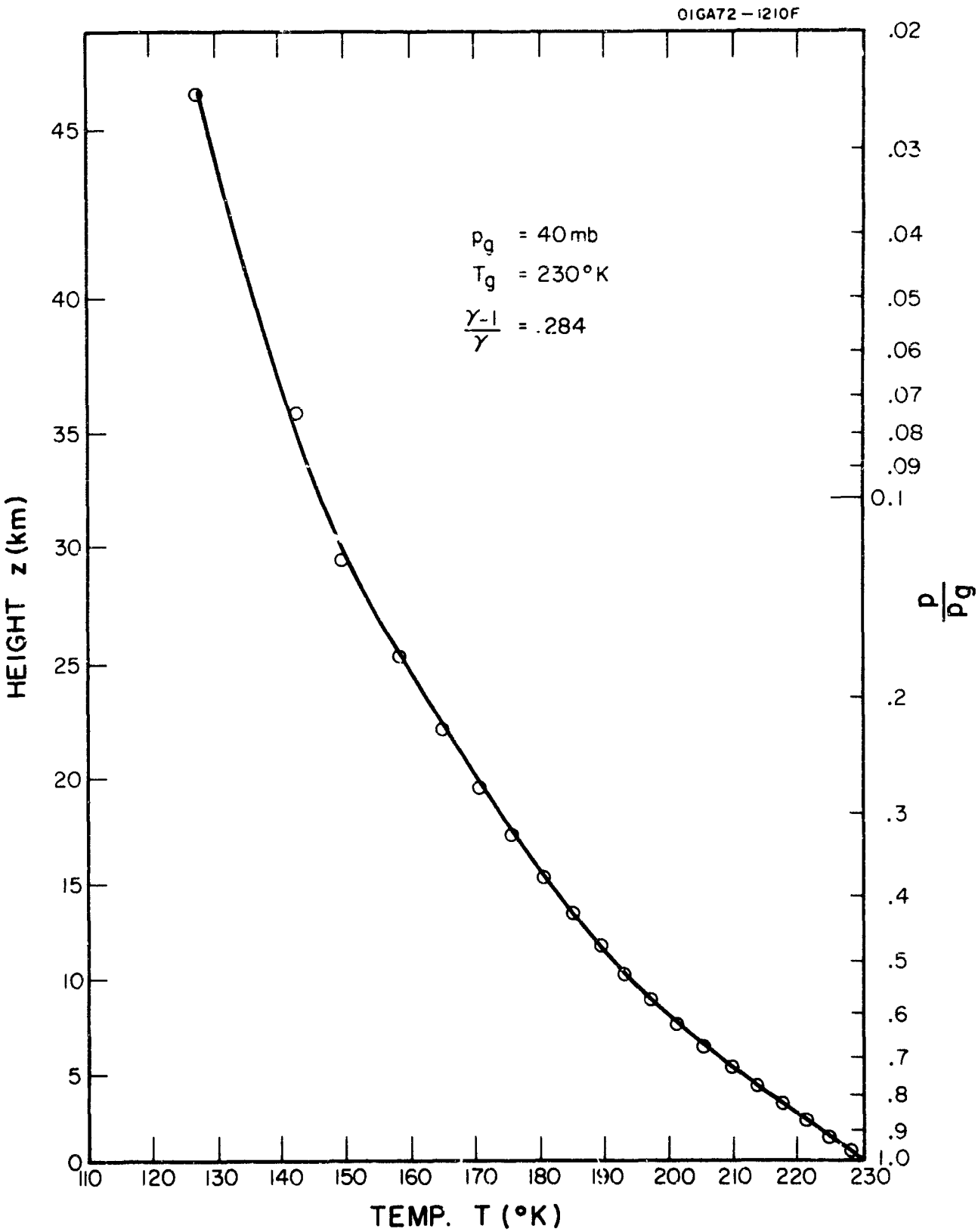

Figure 4. Vertical distribution of temperature in the Martian atmosphere (Physical Model 3).

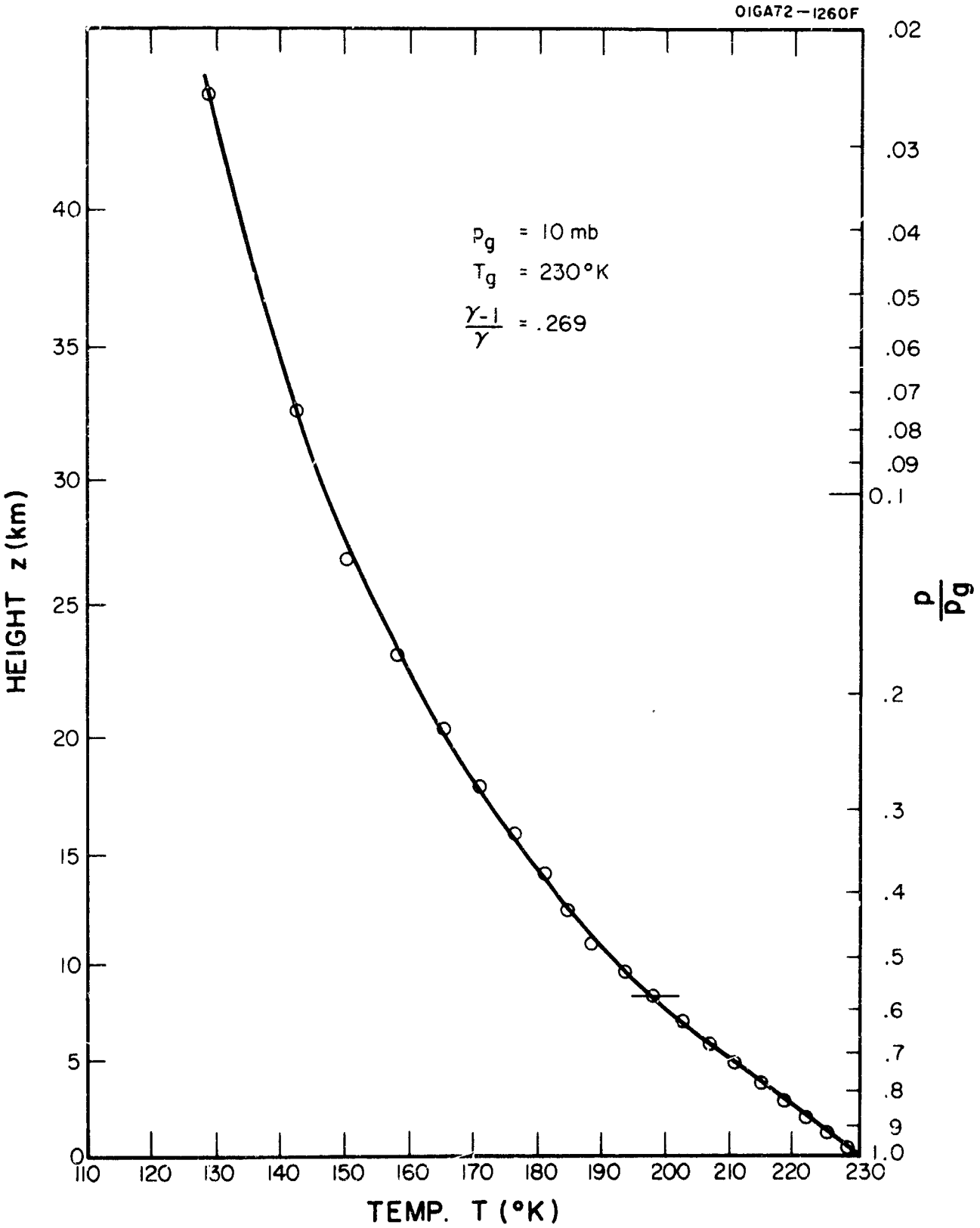

Figure 5. Vertical distribution of temperature in the Martian atmosphere (Physical Model 4).

To determine the effect of different surface temperatures on the temperature profile, computations were performed with the 25-mb model for two extreme surface temperatures — 200°K and 300°K. This temperature range should cover average seasonal and latitudinal variations of Martian surface temperature. The results of these computations are shown in Figures 6 and 7. In the 200°K case, the tropopause is at about 6 km; in the 300°K case, at about 17 km. The increase of tropopause height with increasing surface temperature is in agreement with results obtained previously with a simple model to determine tropopause height in the Martian atmosphere [5]. This variation of tropopause height with surface temperature suggests that the equatorial tropopause on Mars may be significantly higher than the polar tropopause. Another interesting feature of these two profiles is the fact that the temperatures of the uppermost layers — 116°K in the 200°K surface temperature case and 151°K in the 300°K surface temperature case — are only about 35°K apart, despite a 100°K difference in surface temperature. The difference in temperature in a height-for-height comparison is somewhat larger due to the fact that the hotter atmosphere (300°K surface temperature) is significantly thicker than the cooler atmosphere (200°K surface temperature).

To investigate the effect of a possible sub-adiabatic lapse-rate in the Martian troposphere, calculations were performed with the 25-mb model for a tropospheric lapse-rate equal to 0.65 of the adiabatic lapse-rate. The average tropospheric lapse-rate in the Earth's atmosphere is about 0.65 times the adiabatic lapse-rate. It is established as a result of moist convection and attendent release of latent heat of condensation. In the Martian atmosphere, in which water vapor is scarce and clouds rarely occur, a tropospheric lapse-rate of 0.65 times the adiabatic is probably a limiting one for the average tropospheric lapse-rate. The limiting lapse-rate in the other direction is the adiabatic lapse-rate. Thus, computations with these two lapse-rates should bracket possible temperature profiles in the Martian atmosphere. The results of the computation with a sub-adiabatic lapse-rate are shown in Figure 8. As one would expect, the tropopause — at about 30 km — is much higher when the tropospheric lapse-rate is sub-adiabatic. Despite this large difference in the height of the tropopause, the temperatures at any level do not differ by more than 15°C from the adiabatic case to the sub-adiabatic case.

To investigate the effect of a non-uniform carbon dioxide mixing ratio with altitude, computations were performed for a case in which the carbon dioxide mixing ratio decreases linearly from the lowest layer to the highest layer by one order of magnitude. Such a vertical distribution might result from the condensation of carbon dioxide in the upper Martian stratosphere. (The condensation temperature of carbon dioxide is 139°K at a pressure of 1 mm of mercury). A surface pressure of 25 mb, total carbon dioxide content of 55 m STP, and 10-layer model are used in this computation. The resulting temperature profile is shown in Figure 9.

The profile is characterized by an extremely high and relatively sharp tropopause at about 30 km and an upper stratosphere temperature of 129°K. Comparing this profile with those of physical models 1-4, it is quite obvious that the temperature profile is more sensitive to the vertical distribution

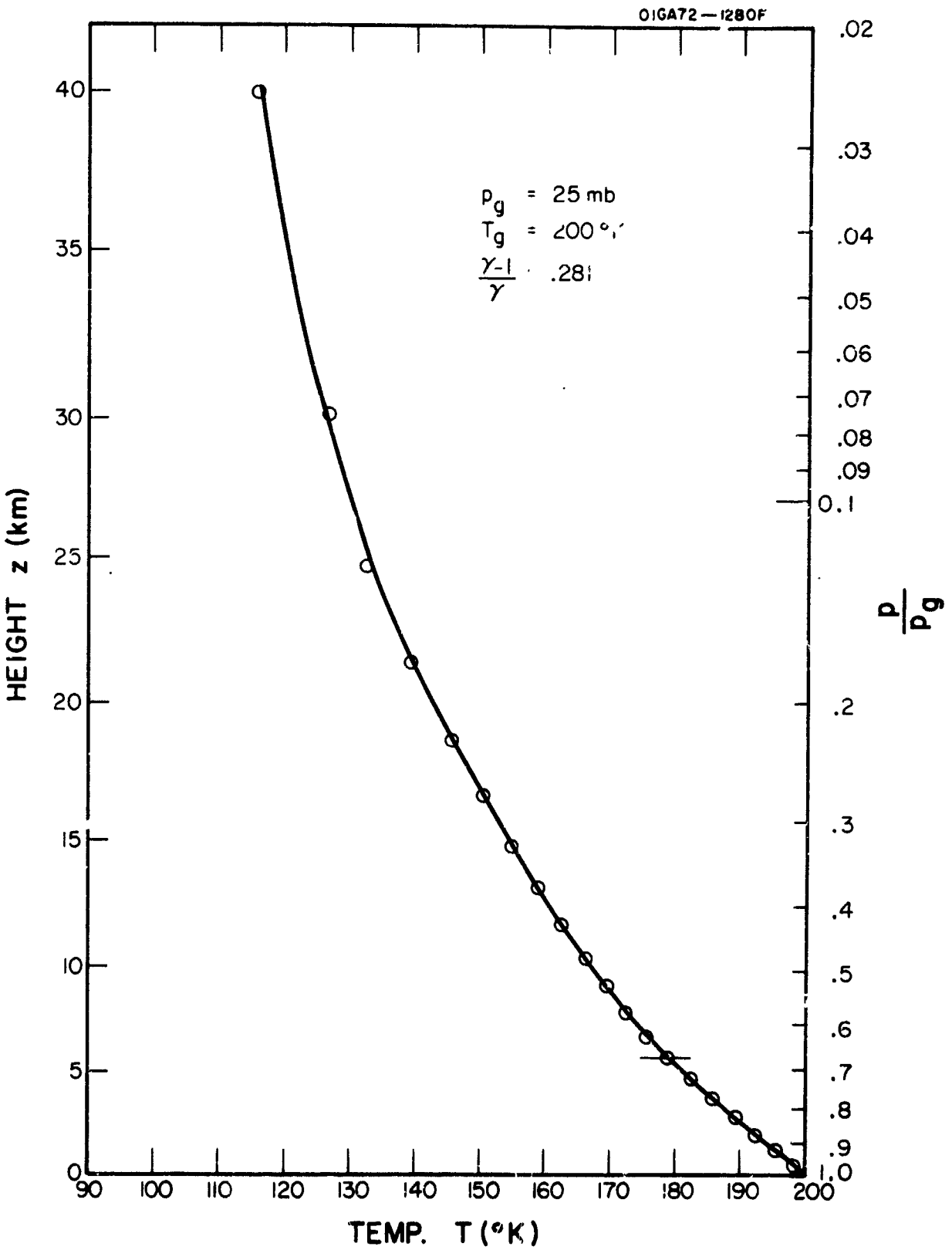

Figure 6. Vertical distribution of temperature in the Martian atmosphere (Physical Model 5).

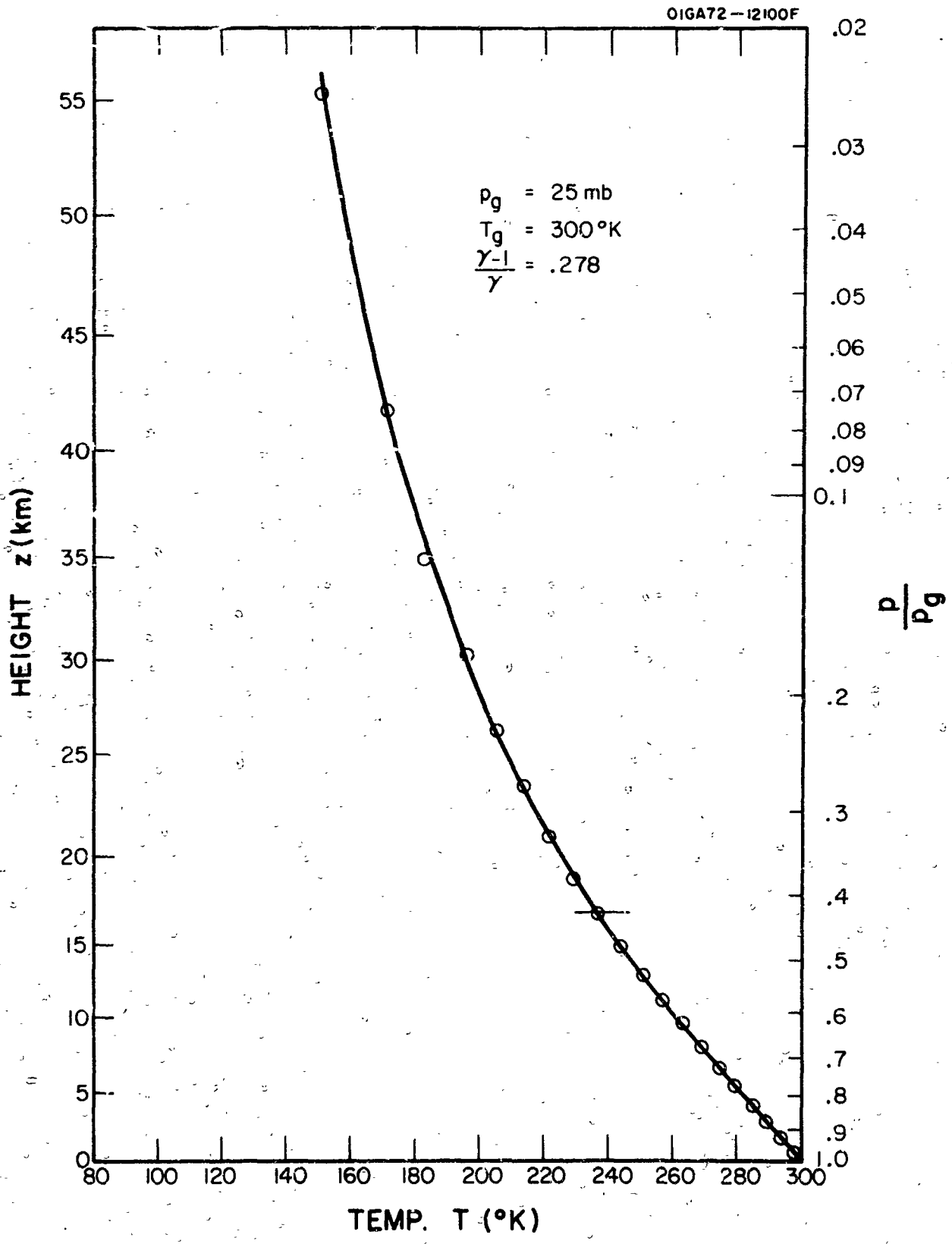

Figure 7. Vertical distribution of temperature in the Martian atmosphere (Physical Model 6).

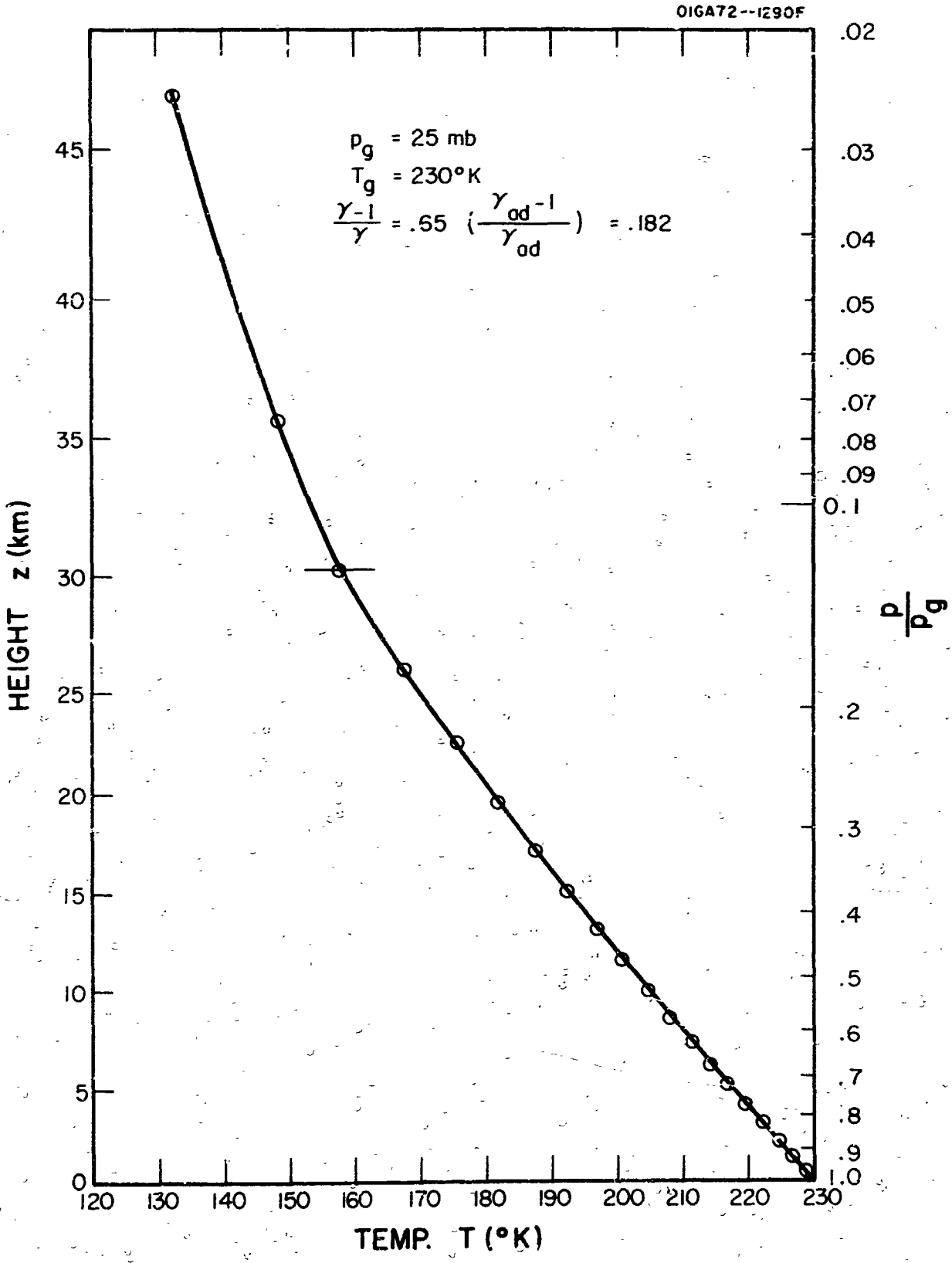

Figure 8. Vertical distribution of temperature in the Martian atmosphere (Physical Model 7).

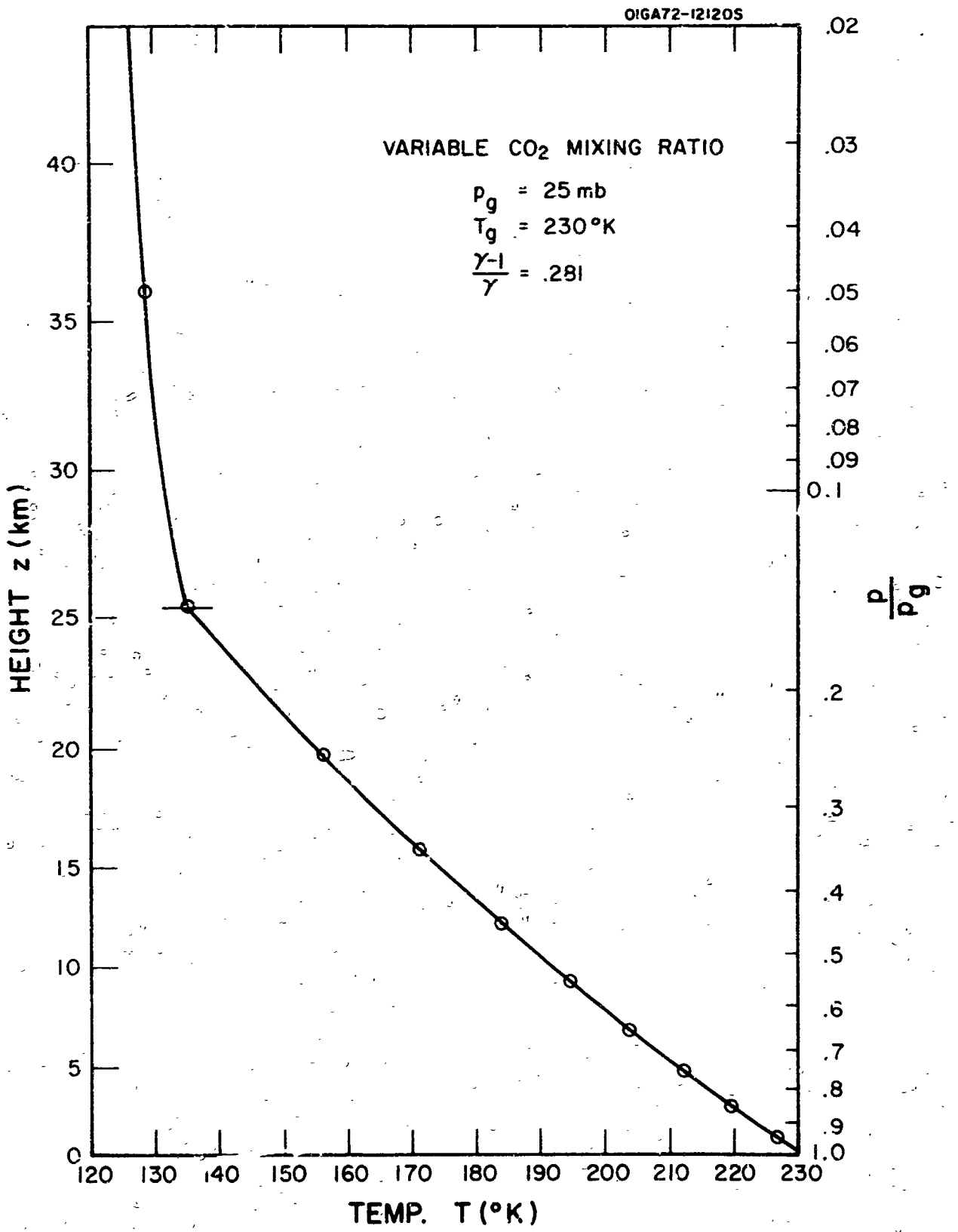

Figure 9. Vertical distribution of temperature in the Martian atmosphere (Physical Model 8).

of carbon dioxide than to the uncertainty of a factor of four in pressure corrected carbon dioxide path length. It was not possible to attain the cut-off criterion of 0.05°K/day for the radiative equilibrium region in this computation, possibly due to the relatively large curvature of the profile in the vicinity of the tropopause, which would cause errors in the linear interpolation schemes used in the computations. A cut-off value of 0.1°K/day was, therefore, used in this computation. Even with this grosser criterion, the variability of the net flux of radiation with height is only of the order of 5×10^{-4} of the net flux.

To investigate the effect of atmospheric absorption of solar radiation on the temperature profile, calculations were performed with the 25-mb model using three assumptions on absorbing constituents. In the first case, it is assumed that only carbon dioxide (55 m STP) is present in the atmosphere; in the second case carbon dioxide (55 m STP) and 10^{-3} cm precipitable water vapor are present; and, in the third case, carbon dioxide (55 m STP) and 10^{-2} cm precipitable water are present. In Figure 10, the heating rates due to carbon dioxide are compared with the heating rates due to water vapor. For the amount of water vapor currently thought to be present in the Martian atmosphere – $\sim 10^{-3}$ prec. cm – the water vapor heating rates are at least one order of magnitude lower than the carbon dioxide heating rates. Even with 10^{-2} prec. cm of water vapor, the water vapor heating rates are significantly lower than the carbon dioxide heating rates. Thus, one would expect the effect of carbon dioxide heating on the temperature profile to be much greater than the effect of water vapor heating. This is borne out by the computed temperature profiles, which are shown in Figure 11. For the case of carbon dioxide alone (profile 9) the temperatures at the top of the atmosphere are almost 17°K higher than in the similar model in which absorption of solar radiation is neglected. With carbon dioxide and 10^{-3} prec. cm of water vapor (profile 10), the temperature is further increased – but only by about 2°K at the top of the atmosphere. With carbon dioxide and 10^{-2} prec. cm of water vapor (profile 11), there is an additional increase of a few degrees. Thus, inclusion of heating due to absorption of solar radiation by carbon dioxide adds almost 17°K to the temperatures computed with a model that neglects solar heating. The combined effect of heating due to carbon dioxide and 10^{-3} prec. cm of water vapor is to raise the upper stratosphere temperatures by about 20°K from their values in a model that neglects solar heating. Inclusion of solar heating also reduces the height of the tropopause. Although, for clarity, only one tropopause is indicated in Figure 11, at about 5 km, the actual height of the tropopause is about 5 km for the carbon dioxide case and for the carbon dioxide plus 10^{-3} prec. cm of water vapor case, and about 4 km for the carbon dioxide plus 10^{-2} prec. cm water vapor case. These values are 2 to 3 km less than in the corresponding case in which solar heating is neglected.

Based upon present indications of carbon dioxide and water vapor content, surface pressure and surface temperature, it is suggested that profile 10 in Figure 11 be used as a tentative estimate of the average vertical distribution of temperature in the Martian atmosphere.

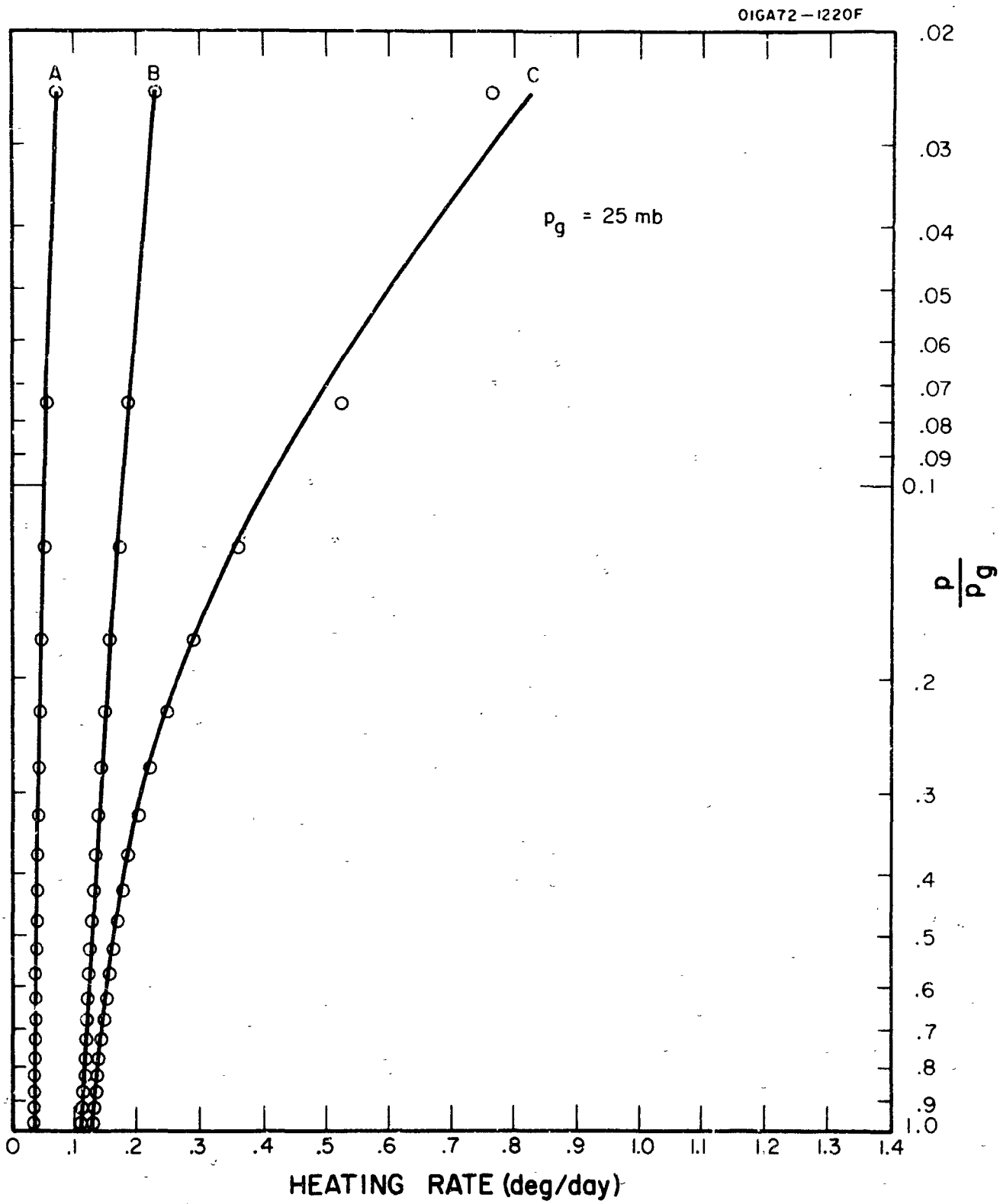

Figure 10. Comparison of computed carbon dioxide and water vapor solar heating rates;
A: H_2O (10^{-3} prec cm) B: H_2O (10^{-2} prec cm)
C: CO_2 (55m STP)

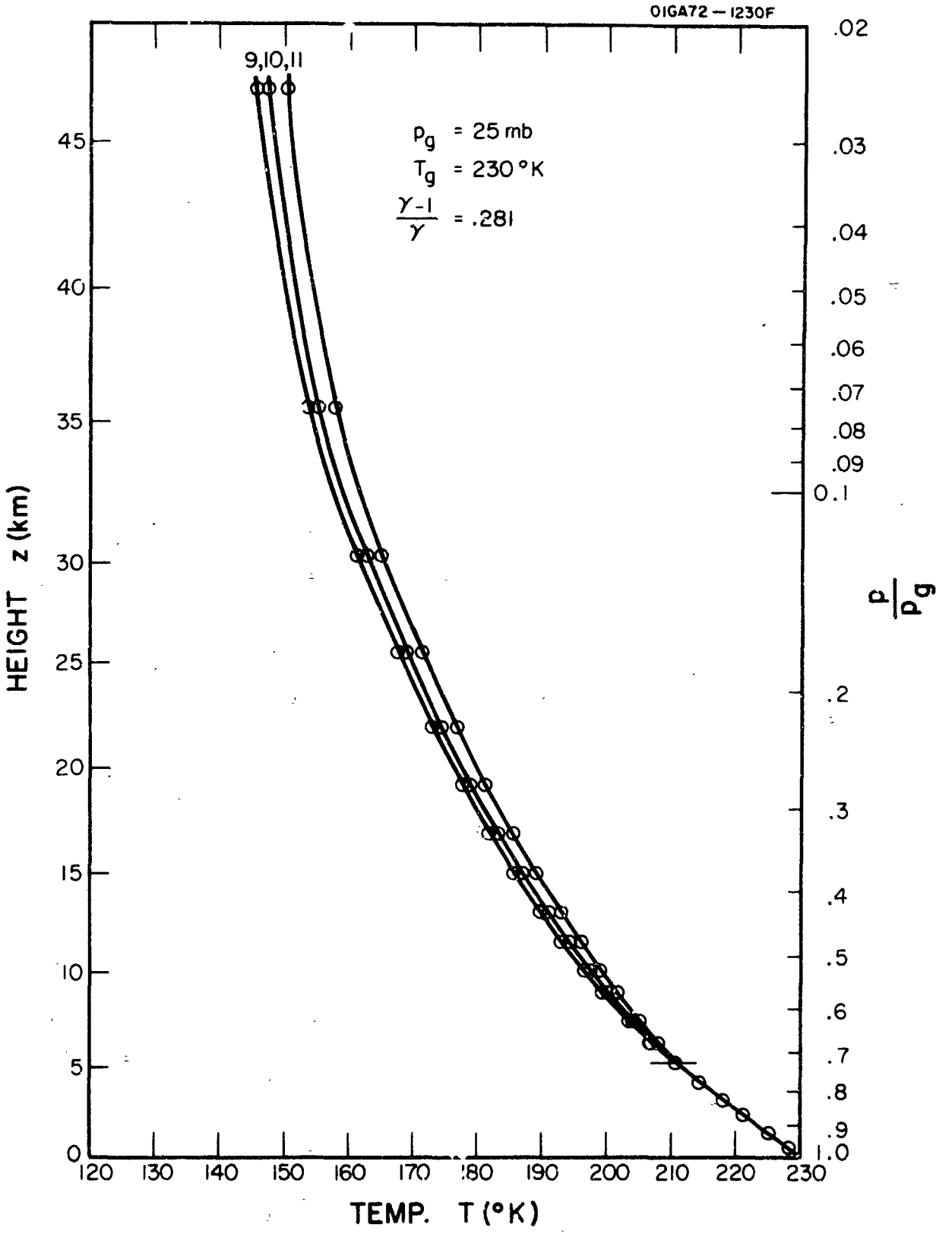

Figure 11. Vertical distributions of temperature in the Martian atmosphere for models in which solar heating is included (Physical Models 9, 10 and 11).

All the computed profiles are presented in one diagram in Figure 12. This diagram illustrates the spread in temperature and tropopause heights obtained with the different models. For clarity only an average tropopause height is indicated for profiles 1-4 and for profiles 9-11. The height scale on this diagram corresponds to profile 7, which is the sub-adiabatic case. The extreme profiles are the ones with surface temperatures of 200°K and 300°K, suggesting that, of the parameters investigated, the surface temperature has the greatest effect on the computed temperature profile.

In all the computations, it was assumed that the effect on the temperature profile of infrared cooling due to water vapor could be neglected. This assumption was based upon comparison of the magnitudes of infrared cooling rates for carbon dioxide and water vapor. Infrared cooling rates were computed for two water vapor amounts — 10^{-2} prec. cm and 10^{-3} prec. cm — and one carbon dioxide amount — 55 m STP — for an isothermal atmosphere with a temperature of 230°K and surface pressure of 25 mb. For these low water vapor amounts, Elsasser's [10] table of R (u, T) had to be extrapolated to lower path lengths. This extrapolation was performed by simply extending Elsasser's values graphically. Thus, the resulting water vapor cooling rates are somewhat uncertain. However, for the present comparison, they are probably of sufficient accuracy. The results of these computations are shown in Table 5. The average carbon dioxide cooling rate is about 2.5 times the average water vapor cooling rate for the large water vapor amount and about 8 times greater in the case of the smaller water vapor amount. It should be remembered that the smaller water vapor amount - 10^{-3} prec. cm — is probably the actual amount in the Martian atmosphere. Furthermore, the ratio of the carbon dioxide cooling rates to the water vapor cooling rates is even higher in the upper layers of the atmosphere. Since the temperature profile in the upper part of the atmosphere is controlled by radiation, while in the lower atmosphere it is limited to the convective lapse-rate, the fact that the carbon dioxide cooling rates are so much greater than the water vapor cooling rates suggests that inclusion of infrared cooling due to water vapor would have a negligible effect on the computed temperature profile. Verification of this reasoning must await actual computations that include the effect of infrared cooling due to water vapor.

Possible diurnal variations in the Martian temperature profile have not been studied in the present research program. The observations of Martian surface temperature suggest values as high as 100°K for the diurnal temperature range at the surface. A complete solution to the problem of day-night variations in the atmospheric temperature profile requires consideration of the non-steady state case and must include the effects of eddy transfer of heat from the Martian surface to the atmosphere. Unfortunately, nothing is known about eddy exchange coefficients for the Martian atmosphere. A previous study [5] indicates that the height at which the amplitude of the diurnal temperature variation reaches one-tenth of its surface value ranges from 1 km to 10 km depending upon the assumed coefficient of eddy thermal conductivity. A complete model of the diurnal variation of the temperature profile should include both the effects of radiative and turbulent heat transfer mechanisms.

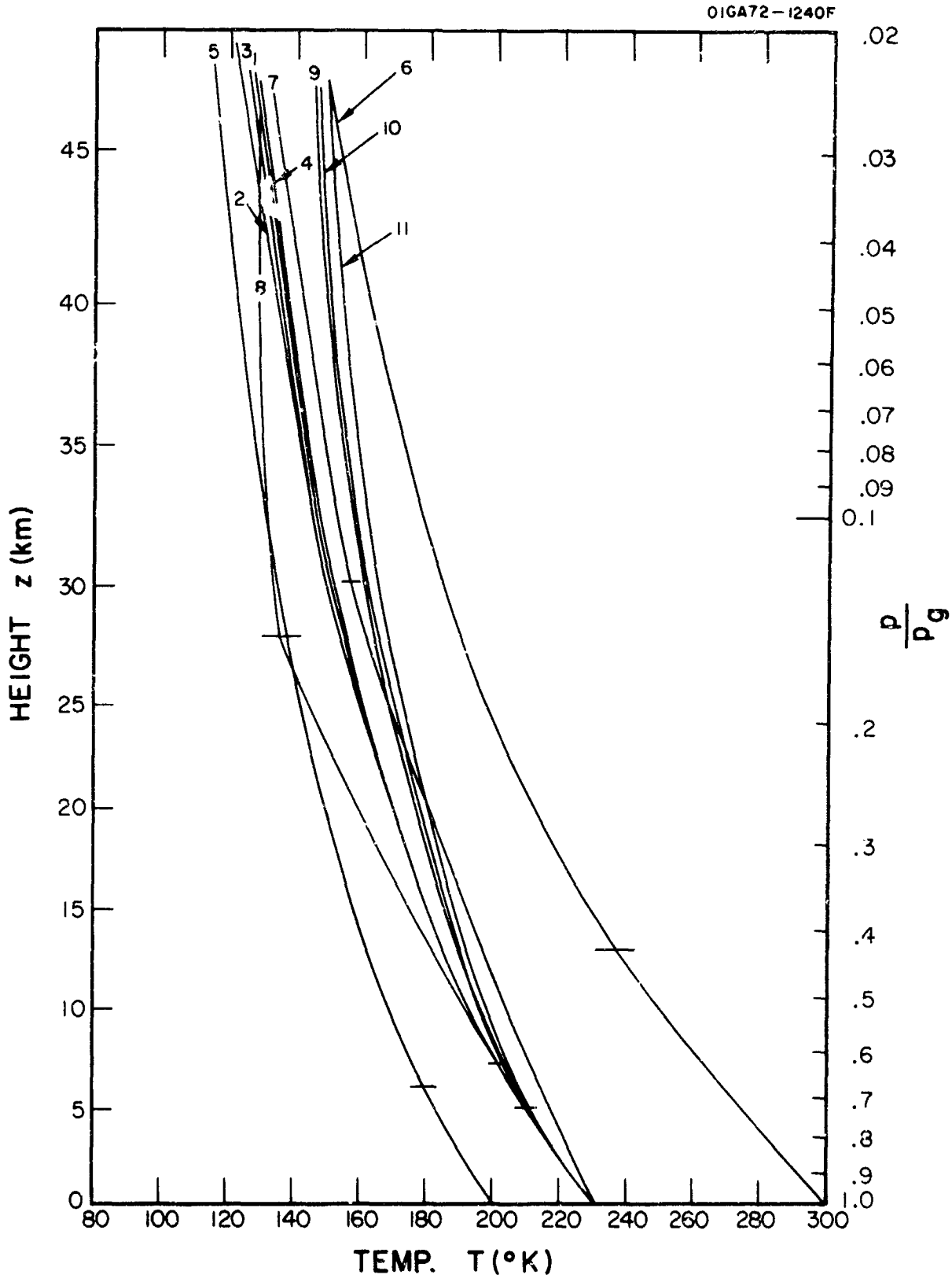

Figure 12. Vertical distributions of temperature in the Martian atmosphere for all physical models (height scale computed with use of temperature distribution of sub-adiabatic Model 7).

TABLE 5

COMPARISON OF COMPUTED INFRARED COOLING RATES (^{o}C/DAY) FOR CARBON DIOXIDE AND WATER VAPOR

(Isothermal Atmosphere at 230^{o}K; p_g = 25 mb)

p (mb)	CO_2 (55 m STP)	H_2O (10^{-2} prec. cm)	H_2O (10^{-3} prec. cm)
23.75	0.8	1.4	0.6
21.25	0.9	1.3	0.4
18.75	1.0	1.4	0.5
16.25	1.2	1.3	0.4
13.75	1.4	1.4	0.5
11.25	1.7	1.4	0.5
8.75	2.2	1.5	0.4
6.25	3.4	1.5	0.3
3.75	5.9	1.4	0.4
1.25	13.8	1.1	0.4

The effect of horizontal transport of heat on the average temperature profile in the Martian atmosphere should be small. Such transports should act mainly to reduce the temperatures of a radiative equilibrium temperature profile computed for the Martian equatorial region and to increase the temperatures of a radiative equilibrium profile computed for the Martian polar regions. The planetary average vertical temperature profile is probably close to the one computed here. The average Martian equatorial and polar temperature profiles may also be close to those computed here for the models with surface temperatures of 300°K and 200°K, respectively, because these surface temperatures may be close to the actual surface temperatures and, hence, already include the effect of horizontal heat transport. (It should be remembered, however, that the temperature profiles computed with the 300°K and 200°K surface temperatures neglect solar heating; as we saw in the models in which solar heating was included, the stratospheric temperatures are increased when this effect is included.)

BLANK PAGE

CONCLUSIONS

On the basis of a combined convective-radiative equilibrium model, vertical temperature profiles for the Martian atmosphere are computed for a number of physical models. The model assumes a radiative equilibrium stratosphere overlying a convective equilibrium troposphere. The computations indicate that the present uncertainty in the Martian surface pressure (estimates of surface pressure range from 10 mb to 85 mb) and carbon dioxide amount (36 m STP to 83 m STP) do not appreciably affect the computed temperature profile, which is characterized by a tropopause at about 7 km and upper stratosphere temperatures of $125^{\circ}K$ to $130^{\circ}K$.

An analysis of the effect of different assumed surface temperatures reveals that a $100^{\circ}K$ difference in assumed surface temperature — $200^{\circ}K$ versus $300^{\circ}K$ — leads to only a $35^{\circ}K$ difference in computed temperature for the upper atmospheric layers. The height of the tropopause varies from 17 km for the $300^{\circ}K$ surface temperature to 6 km for the $200^{\circ}K$ surface temperature.

Computations with two different convective lapse-rates — the adiabatic lapse-rate and 0.65 times the adiabatic lapse-rate — which are probably extreme values for the average tropospheric lapse-rate on Mars, lead to temperature profiles that do not differ by more than $15^{\circ}K$ at any level. However, the height of the tropopause increases to about 30 km for the sub-adiabatic lapse-rate.

The effect of a variable carbon dioxide mixing ratio with altitude is analyzed with the aid of a model in which the carbon dioxide mixing ratio decreases linearly from the lowest atmospheric layer to the highest by one order of magnitude. The total amount of carbon dioxide is maintained at 55 m STP. The computed height of the tropopause is about 30 km. An upper stratosphere temperature of about $129^{\circ}K$ is obtained. This result suggests that the vertical temperature profile is more sensitive to a possible vertical variation of carbon dioxide mixing ratio than to variations in total carbon dioxide reduced path length arising from present uncertainties in total carbon dioxide amount and surface pressure.

Inclusion of the effect of atmospheric absorption of solar radiation raised the upper stratospheric temperatures about $20^{\circ}K$ above the values computed with a model that neglects solar heating. The height of the tropopause is reduced by about 2 km to a height of 5 km.

A sample calculation comparing carbon dioxide and water vapor infrared cooling rates suggests that infrared radiative transfer due to water vapor can be neglected in computations of the temperature profile, if the total amount of water vapor is of the order of 10^{-3} prec. cm or less.

For present uncertainties in the correct physical model to be used for the Martian atmosphere, the results indicate that the computed temperature profiles show relatively little variability. Although the height of the tropopause varies considerably from model to model, the vertical temperature profile is not particularly sensitive to these variations since the lower stratospheric temperature lapse rates are not too different from the tropospheric lapse-rates. This situation is completely different from that prevailing in the Earth's atmosphere, where there is generally a large change in the lapse-rate at the tropopause.

A tentative model of the average vertical distribution of temperature in the Martian atmosphere is suggested. This temperature profile is based upon computations with an assumed surface pressure of 25 mb, carbon dioxide amount of 55 m-STP, water vapor amount of 10^{-3} prec. cm, adiabatic lapse-rate in the troposphere, and surface temperature of 230°K. The effects of infrared cooling due to carbon dioxide and solar heating due to carbon dioxide and water vapor are considered. The suggested temperature profile (profile 10, Figure 11) is characterized by a tropopause at a height of about 5 km. In the Martian stratosphere, the temperature continues to decrease with height to a value of about 145°K above 45 km.

REFERENCES

1. Kaplan, L. D., Munch, G. and Spinrad, "An Analysis of the Spectrum of Mars" Astroph. J., 139, 1-15 (1964).

2. Manabe, S. and Strickler, R. F., "Thermal Equilibrium of the Atmosphere with Convective Adjustment," J. Atmos. Sci., 21, 361-385 (1964).

3. Hess, S., "Some Aspects of the Meteorology of Mars," J. Meteor., 7, 1-13 (1950).

4. Goody, R., "The Atmosphere of Mars," Weather, 12, 3-15 (1957).

5. Ohring, G. and Cotè, O, "The Meteorology of Mars and Venus," GCA Technical Report No. 63-6-N, Contract No. NASw-286 (1963).

6. Schilling, G. F., "Limiting Model Atmospheres of Mars," JPL Report R-402-JPL (1962).

7. Evans, D. C. and Wasko, P. E., "Model Atmospheres for the Planet Mars," Douglas Aircraft Report SM-44552 (1963).

8. Levin, G. M, Evans, D. E. and Stevens, V., "NASA Engineering Models of the Mars Atmosphere for Entry Vehicle Design," NASA Technical Note TN D-2525 (1964).

9. Ohring, G., "A Theoretical Estimate of the Average Vertical Distribution of Temperature in the Martian Atmosphere." Icarus, 1, 328-333 (1963).

10. Elsasser, W. M., "Atmospheric Radiation Tables," AMS Meteorological Monographs, 4 No. 23 (1960).

11. Roach, W. T., "The Absorption of Solar Radiation by Water Vapor and Carbon Dioxide in a Cloudless Atmosphere," Quart. J. Roy. Met. Soc., 87, 364-373 (1961).

12. Howard, J. N., Burch, D. L. and Williams, D., "Near Infrared Transmission through Synthetic Atmospheres," G.R.P. 40 (Astia AD-87679) (1955).

BLANK PAGE

APPENDIX A

DERIVATION OF EQUATIONS FOR UPWARD AND DOWNWARD INFRARED RADIATION FLUXES

The downward and upward fluxes of infrared radiation at an atmospheric level u_o can be written as (see, for example, Reference A1)

$$F\downarrow (u_o) = \int_{\Delta\nu} d\nu \int_{u_o}^{u_1} B_\nu \frac{\partial \tau_F(u-u_o)}{\partial u} du \qquad (A1)$$

$$F\uparrow (u_o) = \int_{\Delta\nu} B_{\nu_g} \tau_F (u_o) d\nu + \int_{\Delta\nu} \int_{o}^{u_o} B_\nu \frac{\partial \tau_F(u_o-u)}{\partial u} du\, d\nu \qquad (A2)$$

where u is the reduced path-length increasing upwards from a value of zero at the ground to u_1 at the top of the atmosphere, ν is wave-number, B_ν is the blackbody flux per unit spectral interval, the subscript g refers to the ground, and τ_F is the flux transmissivity per unit spectral interval. The spectral integration extends over an atmospheric absorption band.

Integrating the second integral in Equation (A1) by parts, we have

$$\int_{u_o}^{u_1} B_\nu \frac{d\tau_F(u-u_o)}{du} du = \left| B_\nu \tau_F (u-u_o) \right|_{u_o}^{u_1} - \int_{u_o}^{u_1} \frac{dB_\nu}{du} \tau_F (u-u_o)\, du \qquad (A3)$$

Since, in the atmosphere, u is a function of T, we can write

$$u = u(T) \text{ and } \frac{d}{du} = \frac{d}{dT}\frac{dT}{du} .$$

Therefore, Equation (A3) can be written as

$$\int_{u_o}^{u_1} B_\nu \frac{d\tau_F(u-u_o)}{du} du = \left| B_\nu \tau_F (u-u_o) \right|_{T_o}^{T_1} - \int_{T_o}^{T_1} \frac{dB_\nu}{du} \tau_F (u-u_o)\, dT \qquad (A4)$$

Define a function

$$Q(u,T) = \int_{\Delta\nu} \frac{dB_\nu(T)}{dt} \tau_F(u)\, d\nu \qquad \text{(A5)}$$

Substituting (A4) and (A5) into (A1), we find

$$F\downarrow(u_o) = -\left| \int_{\Delta\nu} B_\nu \tau_F (u-u_o)\, d\nu \right|_{T_o}^{T_1} + \int_{T_o}^{T_1} Q(u-u_o,T)\, dT \qquad \text{(A6)}$$

Equation (A6) can be written as

$$F\downarrow(u_o) = -\int_{\Delta\nu} B_\nu(T_1)\, \tau_F(u_1-u_o)\, d\nu + \int_{\Delta\nu} B_\nu(T_o)\, \tau_F(o)\, d\nu + \int_{T_o}^{T_1} Q(u-u_o,T)\, dT \qquad \text{(A7)}$$

Making use of the definition of Q, we can write

$$\int_{\Delta\nu} B(T_i)\, \tau_F[u(T_i)]\, d\nu = \int_{\Delta\nu} \tau_F[u(T_i)] \int_o^{T_i} \frac{dB_\nu}{dt}\, dT\, d\nu = \int_o^{T_i} Q[u(T_i),T]\, dT \qquad \text{(A8)}$$

where T_i is the temperature at the level $u(T_i)$.

Substituting (A8) into (A7), we have

$$F\downarrow(u_o) = -\int_o^{T_1} Q(u_1-u_o,T)\, dT + \int_o^{T_o} Q(0,T)\, dT + \int_{T_o}^{T_1} Q(u-u_o,T)\, dT \qquad \text{(A9)}$$

Without any loss of generality u_o can be replaced by zero. Equation (A9) can be re-written as

$$F\downarrow (u_o) = \int_o^{T_o} Q\ (0,T)\ dT + \int_{T_o}^{T_1} Q\ (u,T)\ dT + \int_{T_1}^{o} Q(u_1,T)\ dT \qquad (A10)$$

The function R (u,T) is defined by the following expressions:

$$Q\ (u,T) = \frac{dB}{dT} - R\ (u,T)$$

$$R\ (u,T) = \int_{\Delta\nu} \frac{dB_\nu}{dT}\ [1 - \tau_F(u)]\ d\nu \qquad (A11)$$

Substituting (A11) into (A10) we find

$$F\downarrow (0) = \int_o^{T_o} \left[\frac{dB}{dT} - R\ (0,T)\right] dT + \int_{T_o}^{T_1} \left[\frac{dB}{dT} - R(u,T)\right] dT$$

$$+ \int_{T_1}^{o} \left[\frac{dB}{dT} - R\ (u_1,T)\right] dT \qquad (A12)$$

Equation (A12) reduces to

$$F\downarrow (0) = -\int_o^{T_o} R\ (0,T)\ dT - \int_{T_o}^{T_1} R\ (u,T)\ dT - \int_{T_1}^{o} R\ (u_1,T)\ dT \qquad (A13)$$

Since R (0,T) is zero, we obtain

$$\boxed{F\downarrow (0) = \int_{T_1}^{T_o} R\ (u,T)\ dT + \int_o^{T_1} R\ (u_1,T)\ dT} \qquad (A14)$$

Equation (A14) is used in the compution of the downward infrared radiation fluxes.

The equation for the upward flux of radiation, (A2), becomes, after integration by parts and making T the independent variable,

$$F\uparrow (u_o) = \int_{\Delta\nu} B_{\nu_g} \tau_F (u_o)\, d\nu + \left| \int_{\Delta\nu} B_\nu \tau_F (u_o - u)\, d\nu \right|_{T_g}^{T_o}$$

$$- \int_{T_g}^{T_o} \frac{dB_\nu}{dT} \tau_F (u_o - u)\, dT \qquad \text{(A15)}$$

Substituting Q (u,T) into Equation (A15), we obtain

$$F\uparrow (u_o) = \int_o^{T_g} Q (u_o, T)\, dT + \int_o^{T_o} Q (0,T)\, dT - \int_o^{T_g} Q (u_o, T)\, dT$$

$$- \int_{T_g}^{T_o} Q (u_o - u, T)\, dT$$

$$= \int_o^{T_o} Q (0,T)\, dT - \int_{T_g}^{T_o} Q (u_o - u, T)\, dT \qquad \text{(A16)}$$

Again, without loss of generality, u_o can be taken as zero and u can now be assumed to increase downwards from the reference level. Rewriting (A16), we have

$$F\uparrow (o) = \int_o^{T_o} Q (o,T)\, dT - \int_{T_g}^{T_o} Q (u,T)\, dT \qquad \text{(A17)}$$

Substituting R (u,T) into (A17), we find

$$F\uparrow (o) = \int_o^{T_o} \left[\frac{dB}{dT} - R (0,T) \right] dT - \int_{T_g}^{T_o} \left[\frac{dB}{dT} - R (u,T) \right] dT \qquad \text{(A18)}$$

Since R (0,T) equals zero, (A18) reduces to

$$F\uparrow (0) = B_g - \int_{T_o}^{T_g} R\ (u,T)\ dT \qquad \text{(A19)}$$

Since B_g is equal to σT_g^4, where σ is the Stefan-Boltzmann constant, we obtain

$$\boxed{F\uparrow (0) = \sigma T_g^4 - \int_{T_o}^{T_g} R\ (u,T)\ dT} \qquad \text{(A20)}$$

Equation (A20) is used for computing the upward fluxes of infrared radiation.

REFERENCES

APPENDIX A

A-1. Elsasser, W. M., "Atmospheric Radiation Tables," AMS Meteorological Monographs, 4 No. 23 (1960).

APPENDIX B

TABLES OF COMPUTED TEMPERATURES

The tropopause level is indicated by a short arrow. Characteristics of each physical model are given in Table 4.

BLANK PAGE

Model 1			Model 2		
p(mb)	T(°K)	Ht(km)	p(mb)	T(°K)	Ht(km)
25.0	230	0.00	85.0	230	0.00
24.4	228	0.45	82.9	228	0.47
23.1	225	1.3	78.6	225	1.4
21.9	222	2.3	74.4	221	2.4
20.6	218	3.2	70.1	218	3.4
19.4	214	4.2	65.9	214	4.5
18.1	210	5.3	61.6	210	5.6
16.9	206	6.4	→ 57.4	206	6.8
→ 15.6	202	7.6	53.1	201	8.0
14.4	197	8.8	48.9	197	9.3
13.1	194	10.1	44.6	193	10.6
11.9	189	11.5	40.4	189	12.1
10.6	185	13.1	36.1	185	13.8
9.4	181	14.8	31.9	180	15.6
8.1	176	16.7	27.6	175	17.6
6.9	171	18.9	23.4	171	19.9
5.6	165	21.4	19.1	164	22.5
4.4	159	24.5	14.9	158	25.7
3.1	150	28.4	10.6	149	29.7
1.9	143	34.0	6.4	140	35.5
0.6	128	45.0	2.1	124	46.9

Model 3

p(mb)	T(°K)	Ht(km)
40.0	230	0.00
39.0	228	0.46
37.0	225	1.4
35.0	221	2.3
33.0	218	3.4
31.0	214	4.4
29.0	210	5.5
27.0	206	6.6
25.0	201	7.8
23.0	197	9.1
21.0	193	10.4
19.0	190	11.9
17.0	185	13.5
15.0	181	15.3
13.0	176	17.3
11.0	171	19.5
9.0	165	22.1
7.0	158	25.3
5.0	150	29.3
3.0	142	35.0
1.0	127	46.3

Model 4

p(mb)	T(°K)	Ht(km)
10.00	230	0.00
9.75	228	0.37
9.25	225	1.1
8.75	222	1.9
8.25	218	2.7
7.75	215	3.5
7.25	211	4.4
6.75	207	5.3
6.25	203	6.3
5.75	198	7.3
5.25	194	8.7
4.75	190	10.1
4.25	185	11.6
3.75	181	13.3
3.25	176	15.3
2.75	170	17.4
2.25	165	20.0
1.75	158	23.0
1.25	151	26.9
0.75	142	32.5
0.25	129	43.5

Model 5			Model 6		
p(mb)	T(°K)	Ht(km)	p(mb)	T(°K)	Ht(km)
25.0	200	0.00	25.0	300	0.00
24.4	199	0.40	24.4	298	0.59
23.1	196	1.2	23.1	294	1.7
21.9	193	2.0	21.9	289	3.0
20.6	189	2.8	20.6	284	4.2
19.4	186	3.7	19.4	279	5.5
18.1	183	4.6	18.1	274	6.9
→ 16.9	179	5.6	16.9	269	8.4
15.6	176	6.6	15.6	263	9.9
14.4	173	7.7	14.4	257	11.5
13.1	170	8.9	13.1	251	13.2
11.9	166	10.1	11.9	244	15.1
10.6	163	11.4	→ 10.6	236	17.1
9.4	159	13.0	9.4	229	19.3
8.1	155	14.6	8.1	221	21.7
6.9	151	16.5	6.9	214	24.4
5.6	146	18.8	5.6	204	27.5
4.4	140	21.5	4.4	196	31.3
3.1	132	24.9	3.1	183	36.1
1.9	127	29.9	1.9	171	42.8
0.6	116	39.8	0.6	151	55.9

Model 7

p (mb)	T (°K)	Ht (km)
25.0	230	0.00
24.4	229	0.45
23.1	227	1.3
21.9	224	2.3
20.6	222	3.3
19.4	220	4.3
18.1	217	5.4
16.9	214	6.5
15.6	211	7.7
14.4	208	9.0
13.1	205	10.4
11.9	201	11.9
10.6	197	13.5
9.4	192	15.4
8.1	187	17.4
6.9	182	19.7
5.6	175	22.3
4.4	167	25.5
→ 3.1	158	29.6
1.9	148	35.4
0.6	133	46.9

Model 8

p (mb)	T (°K)	Ht (km)
25.0	230	0.00
23.8	227	0.88
21.3	220	2.7
18.8	212	4.8
16.3	204	7.0
13.8	194	9.5
11.3	184	12.3
8.8	171	15.6
6.3	156	19.6
→ 3.8	135	25.2
1.3	129	36.0

Model 9			Model 10		
p(mb)	T(°K)	Ht(km)	p(mb)	T(°K)	Ht(km)
25.0	230	0.00	25.0	230	0.00
24.4	228	0.45	24.4	228	0.45
23.1	225	1.3	23.1	225	1.3
21.9	222	2.3	21.9	222	2.3
20.6	218	3.2	20.6	218	3.2
19.4	214	4.2	19.4	214	4.2
→ 18.1	210	5 3	→ 18.1	210	5.3
16.9	206	6.4	16.9	207	6.4
15.6	203	7.6	15.6	204	7.6
14.4	200	8.8	14.4	201	8.9
13.1	197	10.1	13.1	197	10.2
11.9	193	11.6	11.9	194	11.6
10.6	190	13.2	10.6	191	13.2
9.4	186	15.0	9.4	187	15.0
8.1	182	16.9	8.1	183	17.0
6.9	177	19.2	6.9	179	19.3
5.6	173	21.8	5.6	174	21.9
4.4	167	25.0	4.4	169	25.1
3.1	161	29.2	3.1	163	29.3
1.9	154	35.2	1.9	155	35.4
0.6	146	47.4	0.6	147	47.8

Model 11

p(mb)	T(^{o}K)	Ht(km)
25.0	230	0.00
24.4	228	0.45
23.1	225	1.3
21.9	222	2.3
20.6	218	3.2
→ 19.3	214	4.2
18.1	211	5.3
16.9	208	6.4
15.6	205	7.6
14.4	202	8.9
13.1	199	10.2
11.9	196	11.7
10.6	192	13.3
9.4	189	15.1
8.1	185	17.1
6.9	182	19.4
5.6	176	22.1
4.4	171	25.3
3.1	165	29.6
1.9	158	35.8
0.6	150	48.4

APPENDIX C

PROGRAM TO CALCULATE R(log u, T) FOR CARBON DIOXIDE

Source Deck, Input Format and Comments.

BLANK PAGE

```
C   PROGRAM TO CALCULATE R(LOG(U),T) FOR CARBON DIOXIDE. SOURCE DECK.
      DIMENSION F(26),T(11,8),C(26)
      READ 200,F(1),F(2),F(3),F(4),F(5),F(6),F(7),F(8),F(9),F(10),F(11),F(12)
      READ 200,F(13),F(14),F(15),F(16),F(17),F(18),F(19),F(20),F(21),F(22),F(23)
      READ 200,F(24),F(25),F(26)
      DO 102 I=1,11
  102 READ 201,T(I,1),T(I,2),T(I,3),T(I,4),T(I,5),T(I,6),T(I,7),T(I,8)
      READ 202,C(1),C(2),C(3),C(4),C(5),C(6),C(7),C(8),C(9),C(10),C(11),C(12)
      READ 202,C(13),C(14),C(15),C(16),C(17),C(18),C(19),C(20),C(21),C(22),C(23)
      READ 202,C(24),C(25),C(26)
      READ 203,U,COF
      PUNCH 205,U
      PUNCH 206
  999 READ 203,TE
      SUM=0.0
      FNU=550.
      DO 104 I=1,26
      FNU=FNU+10.
      FNT=(2.5915E-08*(1.4389*FNU)**4)*EXP(1.4389*FNU/TE)
      FNT=FNT/((EXP(1.4389*FNU/TE)-1.)**2*TE*TE)
      FNU2=(FNU-670.)*(FNU-670.)
      IF(12-I)1,2,3
    1 DELL=-3.4E-04*(293.-TE)*FNU2/TE+.43429448*LOG(293./TE)
      GO TO 4
    2 DELL=.43429448*LOG(293./TE)
      GO TO 4
    3 DELL=-4.6E-04*(293.-TE)*FNU2/TE+.43429448*LOG(293./TE)
    4 ARG=U+F(I)+DELL
      IF(ARG+6.) 12,12,13
   12 TAU=0.0
      GO TO 14
   13 IF(ARG-2.) 15,16,16
   16 TAU=1.0
      GO TO 14
   15 IF(ARG) 5,6,7
    5 K=ARG-1.
      FK=-K
      J=(FK+ARG)*10.
```

```
      FJ=J
      FJ=FJ*0.1
      DELTA=(FK-FJ+ARG)*10.
      GO TO 8
    6 J=0
      K=0
      DELTA=0.
      GO TO 8
    7 K=ARG
      FK=K
      J=(ARG-FK)*10.
      FJ=J
      FJ=FJ*0.1
      DELTA=(ARG-FK-FJ)*10.
    8 K=K+7
      J=J+1
      J1=J+1
      TAU=T(J,K)+DELTA*(T(J1,K)-T(J,K))
      TAU=1.-TAU
   14 FNT=FNT*TAU
  104 SUM=SUM+FNT*C(I)
      SUM=SUM*3.3333333
      SUM=SUM*COF
      PUNCH 204,SUM,TE
      GO TO 999
  200 FORMAT(12F4.2)
  201 FORMAT(8F5.4)
  202 FORMAT(12F2.1)
  203 FORMAT(2E10.0)
  204 FORMAT(F6.3,2XF5.0)
  205 FORMAT(6HLOG(U),F7.3)
  206 FORMAT(3X1HR,4X4HTEMP)
      END
```

INPUT FORMAT FOR PROGRAM WHICH CALCULATES R(LOG(U),T) FOR CARBON DIOXIDE.
CARDS 1,1 TO 1,3 LOG(L) FOR CARBON DIOXIDE (ELSASSER(1960), P39 TABLE 8)
CARDS 2,1 TO 2,11 TAU(F) FOR CARBON DIOXIDE ,ELSASSER (1960) P38 TABLE 2)

CARDS 3,1 TO 3,3 CONSTANTS FOR INTEGRATION BY SIMPSONS RULE.
THESE CARDS ARE LISTED BELOW.

```
-497-405-330-263-206-150-105-061-021+016+030+043
+032+000-034-072-100-150-100-227-267-300-352
-393-439-483
10000099520966209024077930530302067002l9
10000099370961508935076140506901773001b3
10000099130956508340074220474601500001b3
09999098970951203739072170441301251000g4
09996098720945508830019970407401020000g3
09993098450939408514067640373100030000g7
09980090140932903390065150338700653000g3
09932097310926008257062530304400512000g1
09974097440918603113059760270700391000g9
09965097040910307959056360233000294000l0
09952096620902407793053030206700219000g2
10402040204020402040204020
25254020402040204020402040
204010
```

CARD 4,1 LOG(U),CORRECTION COEFFICIENT. FORMAT(E10.3,E10.3)

CARDS 5,1. 5,2,...ETC. TEMPERATURES (K).FORMAT(E10.3)

THIS PROGRAM PUNCHES ON CARDS R(LOG(U),T) AS A FUNCTION OF LOG(U) AND TEMPERATURE(K).

"PRECEDING PAGE BLANK-NOT FILMED"

APPENDIX D

PROGRAM FOR COMPUTATION OF TEMPERATURE PROFILES

Source Deck, Input Format and Comments.

```
C    TEMPERATURE DISTRIBUTION, ITERATION METHOD. SOURCE DECK.
       DIMENSION R(13,24),U(13),TMP(20),DELU(20),HR(20)
       DO 10 I=1,13
       DO 10 J=1,24,6
10 READ 100,R(I,J),R(I,J+1),R(I,J+2),R(I,J+3),R(I,J+4),R(I,J+5)
       DO 11 I=1,13
  11 READ 102,U(I)
       READ 102,PG,CA,G,CP,TEEG,N
       PRINT 500,PG,CA,TEEG
       PRINT 501,G,CP,N
       DO 13 I=1,N
   13 READ 102,DELU(I)
       DO 14 I=1,N
   14 READ 102,HR(I)
   40 DO 6 I=1,N
    6 READ 507,TMP(I)
       FN=N
       C2=-G*FN/(CP*PG)
       C3=PG/FN
       ACCEPT 507,DTIME,KIN
       PRINT 503
       PRINT 506
       TBF=TMP(KIN-1)
       DTN=TMP(N-1)-TMP(N)
       TO=TMP(N)-0.5*DTN
       N1=N+1
       DO 300 K=KIN,N1
       FK=K
       IF(K-N1) 29,30,29
   30 BOUND=0.
       GO TO 36
   29 XU=0.
       DO 600 I=K,N
       FI=I
       P=PG+(.5-FI)*C3
  600 XU=XU+P*DELU(I)
       XU=.43429448*LOG(XU)
       EXECUTE PROCEDURE 2
```

```
 36 FDN=BOUND
    FUP=0.
    DO 299 I=1,N
    FI=I
    XT=TMP(I)
    IF(I-1) 21,20,21
 21 IF(I-N) 22,23,22
 20 DT=TEEG-0.5*(TMP(1)+TMP(2))
    GO TO 24
 23 DT=DTN
    GO TO 24
 22 DT=(TMP(I-1)-TMP(I+1))*0.5
 24 XU=0.
    IF(I-K) 26,601,15
601 P=PG+(.5-FI)*C3
    XU=P*.5*DELU(I)
    GO TO 602
 15 IEND=I-1
    DO 603 II=K,IEND
    FII=II
    P=PG+(.5-FII)*C3
603 XU=XU+P*DELU(II)
    P=PG+(.5-FI)*C3
    XU=XU+P*.5*DELU(I)
    GO TO 602
 26 IBEG=I+1
    IEND=K-1
    DO 604 II=IBEG,IEND
    FII=II
    P=PG+(.5-FII)*C3
604 XU=XU+P*DELU(II)
    P=PG+(.5-FI)*C3
    XU=XU+P*.5*DELU(I)
602 XU=.4342944*LOG(XU)
    EXECUTE PROCEDURE 1
    FUP=FUP+ARE*DT
299 CONTINUE
    FNT=-FUP-FDN
```

```
      IF(K-KIN) 27,28,27
   28 FN1=FNT
      GO TO 300
   27 DIVF=FNT-FN1
      FN1=FNT
      K1=K-1
      DLT=C2*DIVF+HR(K1)
      FK1=K1
      T=TMP(K1)+DLT*DTIME
      IF(K1-1) 31,32,31
   32 TADI=TEEG*((FN-.5)/FN)**CA
      GO TO 33
   31 TADI=TBF*((FN-FK1+.5)/(FN-FK1+1.5))**CA
   33 IF(T-TADI) 34,34,35
   35 TADI=T
   34 P=PG+C3*(.5-FK1)
      PRINT 505,P,TMP(K1),T,TADI,DLT
      PUNCH 507,TADI
      TBF=TADI
  300 CONTINUE
      BEGIN PROCEDURE 1
      DO 200 L=1,12
      DF1=XU-U(L)
      DF2=XU-U(L+1)
      SGN=DF1*DF2
      IF(SGN) 201,201,200
  200 CONTINUE
  201 TI=63.
      DO 202 M=1,23
      TI=TI+10.
      TI1=TI+10.
      DF1=XT-TI
      DF2=XT-TI1
      SGN=DF1*DF2
      IF(SGN) 203,203,202
  202 CONTINUE
  203 X1=(R(L,M+1)-R(L,M))*DF1/10.+R(L,M)
      X2=(R(L+1,M+1)-R(L+1,M))*DF1/10.+R(L+1,M)
```

```
      ARE=(X2-X1)*(XU-U(L))/(U(L+1)-U(L))+X1
      END PROCEDURE 1
      BEGIN PROCEDURE 2
      DELLT=(T0-73.)/20.
      BOUND=0.
      XT=73.
      EXECUTE PROCEDURE 1
      BOUND=ARE/2.
      DO 301 J=1,19
      FJ=J
      XT=FJ*DELLT+73.
      EXECUTE PROCEDURE 1
  301 BOUND=BOUND+ARE
      XT=T0
      EXECUTE PROCEDURE 1
      BOUND=BOUND+ARE/2.
      BOUND=BOUND*DELLT
      END PROCEDURE 2
      GO TO 40
  100 FORMAT(F4.3,F4.3,4.3,F4.3,F4.3,F4.3,F4.3)
  102 FORMAT(E10.3,E10.3,E10.3,E10.3,E10.3,I4)
  500 FORMAT(2HPG,E10.3,2X2HCA,E10.3,2X2HTG,E10.3)
  500 FORMAT(2HPG,F10.3,2X2HCU,E10.3,2X2HCA,E10.3,2X2HTG,E10.3)
  501 FORMAT(1HG,E10.3,2X2HCP,E10.3,2X1HN,I4)
503FORMAT(2X5HPRESS2X7HTEMP(T)2X10HTEMP(T+DT)2X10HTEMP(T+DT)3X7HDTMP/DT)
  506 FORMAT(30X11H(CORRECTED))
  505 FORMAT(F6.1,3XF6.1,4XF6.1,3XF6.1,5XE10.3)
  507 FORMAT(F6.1,I4)
      END
```

INPUT FORMAT TO ITERATION PROGRAM

```
CARD 1,1    R(1,1),R(1,2),...,R(1,6)
CARD 1,2    R(1,7),R(1,8),...,R(1,12)
CARD 1,3    R(1,13),R(1,14),...,R(1,18)
CARD 1,4    R(1,19),R(1,20),...,R(1,24)
```

CARD 2,1 R(2,1),R(2,2),...,R(2,6)

.
.
.

CARD 13,4 R(13,13),R(13,14),...,R(13,24)

R(I,J)=R(LOG(U(I)),T(J)) FOR CARBON DIOXIDE, WHERE LOG(U(1))=-2+.7,LOG(U(2))=-1, ...,LOG(U(13))=+2.7, AND T(1)=73K, T(2)=83K,...T(24)=303K. FORMAT F4.3.

CARD 14,1 -1.3
CARD 14,2 -1.0

.
.
.

CARD 14,13 +2.7

CARD 14,I IS LOG(U(I)),I=1,...13. FORMAT E10.3.

CARD 15,1 PG,CA,G.CP,TEEG,N

PG IS PRESSURE AT GROUND (mb), CA IS ADIABATIC CONSTANT, CP IS SPECIFIC HEAT AT CONSTANT PRESSURE (CAL./G./DEG.), TEEG IS TEMPERATURE AT GROUND (K),N IS NUMBER OF LAYERS (MAXIMUM N IS 20), AND G IS ACCELERATION OF GRAVITY (CM./SEC./SEC./1000 - G IS DIVIDED BY 1000 TO CONVERT PRESSURE (mb) TO PRESSURE(DYNES/CM*CM). FORMAT E10.3 FOR PG,CA,G,CP,TEEG, I4 FOR N. THESE QUANTITIES ARE PRINTED AT THE BEGINNING OF THE PROBLEM.

CARD 16,1 DELU(1)
CARD 16,2 DELU(2)

.
.
.

CARD 16,N DELU(N)

DELU(I) IS THE OPTICAL PATH LENGTH OF CARBON DIOXIDE FOR THE I-TH LAYER. THE UNITS OF DELU(I) ARE CM./1000. FORMAT E10.3.

CARD 17,1 HR(1)
CARD 17,2 HR(2)

.
.
.

CARD 17,N HR(N)
HR(I) IS THE SOLAR HEATING RATE (DEG./DAY) AT THE MIDDLE OF THE I-TH LAYER.
FORMAT E10.3.

CARD 18,1 TMP(1)
CARD 18,2 TMP(2)
.
.
.
CARD 18,N TMP(N)
TMP(I) IS THE TEMPERATURE (K) AT THE MIDDLE OF THE I-TH LAYER. FORMAT F6.1.

AFTER CARD 18,N IS READ IN THE PROGRAM TRANSFERS TO THE TYPEWRITER WHERE THE QUANTITIES DTIME AND KIN (FORMAT F6.1,I4) ARE TYPED. DTIME IS THE TIME INTERVAL (DAYS), KIN IS THE NUMBER OF THE LAYER WHERE THE FIRST NEW TEMPERATURE IS TO BE CALCULATED (IF KIN IS NOT 1 THE PROGRAM ASSUMES THAT THE NEW TEMPERATURES OF THE LAYERS BELOW KIN ARE EQUAL TO THE CORRESPONDING READ IN TEMPERATURES. THEREFORE, TEMPERATURES ALREADY KNOWN TO LIE ON THE ADIABATIC CURVE NEED NOT BE RECALCULATED).

DURING EACH ITERATION THE PROGRAM PRINTS THE PRESSURE(M.B.) AT THE MIDDLE OF EACH LAYER(PRESS), AND THE CORRESPONDING READ IN TEMPERATURE (TEMP(T)), THE NEW TEMPERATURE (TEMP(T+DT)), THE ADIABATICALY CORRECTED TEMPERATURE (TEMP(T+DT)-CORRECTED), AND THE RATE OF CHANGE OF TEMPERATURE (DTMP/DT), AND PUNCHES THE ADIABATICALY CORRECTED TEMPERATURE.

AT THE END OF THE ITERATION CYCLE THE PROGRAM TRANSFERS TO THE READ STATEMENT FOR CARDS 18,I WHERE THE PUNCHED TEMPERATURES ARE READ IN FOR THE NEXT ITERATION. THE QUANTITIES DTIME AND KIN ARE THEN TYPED IN.
N.B. IF KIN IS NOT 1, THE PROGRAM WILL NOT PUNCH THE TEMPERATURES FOR THE LAYERS BELOW KIN. THESE TEMPERATURES, TMP(1),...,TMP(KIN-1), SINCE THEY DO NOT CHANGE FROM ITERATION TO ITERATION, CAN BE SUPPLIED FROM A PREVIOUS ITERATION.

APPENDIX E

PROGRAM TO CONVERT PRESSURE TEMPERATURE COORDINATES TO HEIGHT TEMPERATURE COORDINATES

Source Deck, Input Format and Comments.

BLANK PAGE

```
C     PROGRAM TO CONVERT PRESSURE TEMPERATURE COORDINATES TO HEIGHT
C    TEMPERATURE COORDINATES.  SOURCE DECK
      DIMENSION T(20)
   99 READ 100,TB,PB,G,FN
      READ 105,R,CP,A,NA,N
      ALPHA=-G*A/CP
      DO 1 I=1,N
    1 READ 101,T(I)
      PUNCH 102,TB,PB,ALPHA
      PUNCH 103
      FN=N
      DEEP=PB/FN
      P=PB+.5*DEEP
      DO 2 I=1,NA
      P=P-DEEP
       Z=(T(I)-TB)/ALPHA
    2 PUNCH 104,T(I),P,Z
      CST=R/(FN*G)
      NA=NA+1
      DO 3 I=NA,N
      ZO=Z
      PO=P
      P=P-DEEP
      BLURB=(T(I-1)-PO/DEEP*(T(I-1)-T(I)))*LOG(P/PO)
      Z-ZO+CST*(T(I-1)-T(I)-BLURB)
    3 PUNCH 104,T(I),P,Z
      GO TO 99
  100 FORMAT(E10.0,E10.0,E10.0,E10.0)
  101 FORMAT(F6.1)
  102 FORMAT(3HTB=,E10.3,2X3HPB=,F10.3,2X6HALPHA=,E10.3)
  103 FORMAT(1X4HTEMP,4X5HPRESS,5X2HHT)
  104 FORMAT(F6.1,2XF6.2,2X,E10.3)
  105 FORMAT(E10.0,E10.0,E10.0,I5,I5)
      END
```

INPUT FORMAT TO PROGRAM WHICH CONVERTS PRESSURE-TEMPERATURE COORDINATES TO HEIGHT-TEMPERATURE COORDINATES.

CARD 1 TB,PB,G,FM

TB IS TEMPERATURE (K) AT GROUND, PB IS PRESSURE (M.B.) AT GROUND, G IS ACCELERATION OF GRAVITY (CM./SEC./SEC.),AND FM IS THE MOLECULAR WEIGHT OF THE ATMOSPHERIC GAS. FORMAT(E10.3)

CARD 2 R,CP,A,NA,N

R IS THE UNIVERSAL GAS CONSTANT (ERGS/DEG.), CP IS THE SPECIFIC HEAT AT CONSTANT PRESSURE (CAL./G./DEG.), A IS A CONVERSION FACTOR (2.39E-08 CAL./ERG.), NA IS THE NUMBER OF ADIABATIC TEMPERATURES, AND N IS THE TOTAL NUMBER OF TEMPERATURES. THE TEMPERATURE AT THE GROUND, PRESSURE AT THE GROUND, AND ADIABATIC LAPSE RATE ARE PUNCHED ON CARDS FOR EACH PROBLEM.

CARDS 3,1 TO 3,N TEMPERATURE AT 1-ST LAYER,..., TEMPERATURE AT N-TH LAYER.

THIS PROGRAM PUNCHES ON CARDS THE TEMPERATURE (K) WITH THE CORRESPONDING PRESSURE (M.B.) AND HEIGHT (CM.), FOR EACH LAYER.